Pre-concentration of Positron-emitting [^{18}F]Fluoride and Radiosynthesis of Fluoride-based Prosthetic Compounds for PET imaging using Magnetic Droplet Microfluidics (MDM)

by

Somewhere Albacite Fiel

B.Sc., Mindanao State University, 2009

Thesis Submitted in Partial Fulfillment of the
Requirements for the Degree of
Master of Science

in the
Department of Chemistry
Faculty of Science

SIMON FRASER UNIVERSITY

Fall 2014

Approval

Name: **Somewhere Fiel**

Degree: **Master of Science (Chemistry)**

Title: ***Pre-concentration of Positron-emitting [^{18}F]Fluoride and Radiosynthesis of Fluoride-based Prosthetic Compounds for PET imaging using Magnetic Droplet Microfluidics (MDM)***

Examining Committee: **Chair: Robert A. Britton**
Associate Professor

Dr. Paul Li
Senior Supervisor
Professor

Dr. Paul Schaffer
Co-Supervisor
Deputy Head of Nuclear Medicine Division
TRIUMF

Dr. Corina Andreoiu
Supervisor
Assistant Professor

Dr. Tim Storr
Supervisor
Associate Professor
[on parental leave]

Dr. David Vocadlo
External Examiner
Professor
Department of Chemistry
Simon Fraser University

Date Defended/Approved: December 09, 2014

Partial Copyright Licence

Abstract

The radioisotope ^{18}F is often considered the best choice for PET imaging, owing to its desirable chemical and radiochemical properties. However, nucleophilic ^{18}F fluorination of large, water soluble biomolecules, based on C-F bond formation, has been difficult. Thus, several aqueous fluorination approach have been developed which offers significant development in radiopharmaceutical synthesis. Furthermore, since ^{18}F decays rapidly, production of these ^{18}F-labelled compounds requires an automated process to reduce production time, reduce radiation exposure and also minimize transfer of reagents during tracer synthesis to reduce sample transfer loss. Herein, a method called magnetic droplet microfluidics (MDM) has been developed which aims to conduct [^{18}F]fluoride pre-concentration and synthesis of ^{18}F-labeled compound on a microfluidic platform. Using this method, we have demonstrated ^{18}F pre-concentration in a small-volume droplet through the use of anion exchanging magnetic particles. By using MDM, the pre-concentration step took approximately 5 min. and the [^{18}F]fluoride solution was pre-concentrated by 15-fold from a volume of 1 mL to 0.05 mL. After the pre-concentration step, an ^{18}F-labelling reaction was performed on the MDM platform using the S-F bond formation in aqueous conditions to produce an arylsulfonyl [^{18}F]fluoride which can be used as a prosthetic group to label PET targeting ligands. The high radiochemical purity of 95 ± 1% was comparable with 96% which was previously reported using conventional method. In addition, when using MDM, the total synthesis time was improved to 15 min. with lower reagent volumes (50-60 µL) used. The MDM method was also used to produce an ^{18}F-labelled aryltrifluoroborate through B-F bond formation. The synthesis of aryltrifluoroborate compound at low activities (~5 mCi), gave radiochemical purities which were low for both MDM (5.8%) and conventional method (6.0%).

Keywords: magnetic particles; droplet microfluidics; positron emission tomography (PET) imaging; ^{18}F; radiotracer; sulfonyl fluoride; aryltrifluoroborates

Dedication

To my husband:

You're God's greatest gift to me. Thank you for inspiring me to be the best person that I could ever be.

Acknowledgements

I would like to start by thanking my senior supervisor Dr. Paul Li for giving me the opportunity to work in his research group. I appreciate all his guidance, patience and kindness in training me throughout my graduate career. I would also like to thank Dr. Paul Schaffer for accepting me as his student and for all his efforts to help me on my project. I also had a better understanding of the radiochemistry field when I took a radiochemistry course under him. I would also like to thank Dr. Tim Storr and Dr. Corina Andreoiu for their advice and for taking time to review this thesis.

All my radioactive runs would not have been possible without the tremendous help from Dr. Hua Yang who properly trained me to conduct safe and successful runs, who made sure I have all that I need in the lab and who also gave me advice on my project. I would like to thank the rest of TRIUMF PET group for accommodating my requests during my radioactive runs.

I would like to thank the past and present members of Li Research Group in SFU: To Michael Wong for initial implementation of the MDM platform and EDX scan, and to Sangho Lee and Samuel Weng for their initial work on the synthesis of the magnetic particles. I would also like to thank Wen Zhou (from Leznoff Group, SFU) for accommodating me in their lab and gave me access to use the glove bag.

The sulfonyl fluoride precursor in this work was prepared by Dr. James Howard Inkster (former PhD student from the Storr Group (SFU) and TRIUMF) and the aryltrifluoroborate precursor was provided by Dr. David Perrin and his team at the University of British Columbia. I appreciate their help in providing me with these compounds and for answering my queries about the reaction conditions involved.

Including those whom I failed to mention, I would like to express my gratitude to all those, even in their little ways, had contributed and helped me throughout this journey.

Thank You!

Table of Contents

List of Figures

List of Tables

List of Equations

List of Schemes

List of Acronyms

CT	Computed Tomography
DMSO	Dimethyl sulfoxide
EC	Electron Capture
EOB	End of Bombardment
^{18}F	Fluorine-18
HPLC	High Performance Liquid Chromatography
IC50	Half maximal inhibitory concentration
K2.2.2	4,7,13,16,21,24-Hexaoxa-1,10-diazabicyclo[8.8.8]hexacosane (Kryptofix® 2.2.2.)
MRI	Magnetic Resonance Imaging
NOTA	1,4,7-triazacyclononane-N,N',N''-triacetic acid
PET	Positron Emission Tomography
QMA	Quaternary methylammonium
RAD-HPLC	HPLC with Radiochemical detection
UV-HPLC	HPLC with UV-Visible absorbance detection
RCY	Radiochemical Yield
SA	Specific Activity
SiFA-A	p-(di-tert-butyl[^{18}F]fluorosilyl)benzaldehyde
$t_{1/2}$	Half-life

Chapter 1. **Introduction**

1.1. Positron Emission Tomography (PET)

In the diagnosis and treatment of diseases, such as cancer, one needs an imaging technique to visualize and understand functional processes that occurs inside a patient's body. With this understanding, it is possible to detect disease while treatable, to monitor disease progression and to evaluate the patient's response to therapy. Over the years, positron emission tomography (PET) has emerged as the premier choice for functional imaging due to its high sensitivity and spatial resolution (Welch and Redvanly, 2003).

Molecular imaging is defined as the non-invasive visualization of *in vivo* biological processes at the molecular level using specific imaging tracers. (Weissleder and Mahmood, 2001; Ametamey et al., 2008). As a tool for molecular imaging, PET observes the physiological and pathological changes of a disease at the molecular level. This tool is in contrast to conventional diagnostic imaging such as X-ray/Computed Tomography (CT) which studies diseases at the anatomical level. PET scans are read alongside with CT or magnetic resonance imaging (MRI) scans giving both anatomic and metabolic information. The novelty of observing both structures and functions give the unique opportunity to reveal pathways and mechanisms responsible for diseases in living subjects (Massoud and Gambhir, 2007).

1.1.1. Overview of positron emission

A PET system produces functional images by detecting coincident pairs of gamma rays emitted by annihilating positrons (β^+). Positrons are introduced into a human body by radiotracers which carry positron-emitting radionuclides. Positrons are particles of antimatter that are produced upon conversion of a proton (p) to a neutron (n)

in the nucleus. Positron emission typically occurs when the nucleus of a radionuclide is proton rich, that is, the ratio of neutrons to protons in the nucleus is low relative to that of the next stable nuclide (Saha, 2006).This emission process is also associated with the production of a neutrino (υ), and is described according to the nuclear equation below:

$$p \rightarrow n + \beta^{+} + \upsilon_{e}$$

Scheme 1.1 General Equation for Positron Emission

One example is the decay of ^{18}F to ^{18}O wherein a positron is emitted, see Scheme 1.2.

$$^{18}F \rightarrow {}^{18}O + \beta^{+} + \upsilon_{e}$$

Scheme 1.2 ^{18}F decay via positron emission

The energetic positron (β^{+}) loses energy as it moves through matter. When almost all of its energy is lost, the positron collides with a nearby electron and both particles are annihilated and energy is released, see Figure 1.1. This annihilation reaction gives rise to two γ-rays (see Scheme 1.3) and they are emitted in the opposite direction at angles very close to 180° from each other, see Figure 1.1 (Overman et al., 1960). These two gamma-rays (511-keV photons) are then detected as a coincidence event when they nearly strike opposing gamma detectors within 12 milliseconds (Beringer and Montgomery, 1942).

$$\beta^{+} + \beta^{-} \rightarrow 2\gamma$$

Scheme 1.3 Annihilation Reaction of positron (β^{+}) and electron (β^{-})

For positron emission to take place, the parent nuclide should have a mass-energy difference to that of the daughter nuclide of at least 1.022 MeV. This energy difference allows for the generation of two gamma emissions, each of 511 keV. If this minimal energy difference is not met, no positron emission will take place and electron capture (EC) becomes a more likely decay pathway, see Scheme 1.4 (Saha, 2006).

$$p + e^{-} \rightarrow n + \upsilon_{e}$$

Scheme 1.4 General for Electron Capture (EC) Decay

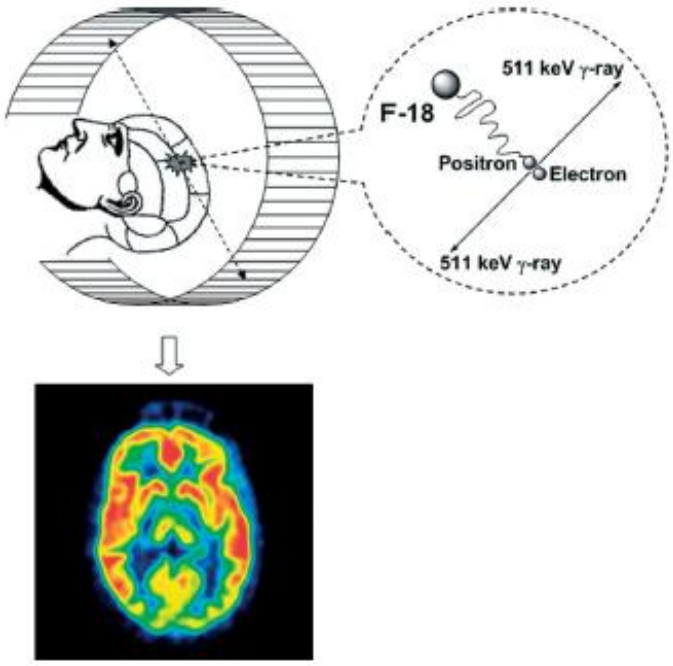

Figure 1.1 Principle of PET imaging, showing a positron and a negative electron annihilate, producing two 511 keV photons travelling in opposite directions

Note: The 511 keV photon was registered by the gamma detector array in the PET imaging system (with permission from Cai et al., 2008).

1.1.2. Gamma detector

Figure 1.2 An image of a PET detector arranged in gamma detector ring

Note: There are 24 detector rings comprising 12,096 scintillation crystals (Sharma et al., 2007).

Gamma detectors are radiation detectors that measure ionizing radiations when they pass through the detector. Interactions between the incident radiation and the detector result in visible photon production, which is then converted into an electrical signal that is processed by downstream electronics. This signal carries the information about: 1) how much energy is deposited on the detector, 2) the physical location of the event in the detector array and 3) the time when the event occurs.

The detectors are generally divided into three categories: gas chambers, semi-conductors and scintillation. The latter one is most commonly used for the detection of gamma photons in PET imaging. The gamma detector consists of an inorganic crystal (scintillator) which emits visible light photons (scintillations) after the interactions of the photons with the crystal (e.g. bismuth germinate or BGO). The rate of photon production is proportional to the energy absorbed by the crystal. The detector is joined to a photomultiplier that convert the light into electrons and then amplify the electrical signal provided by those electrons (Hamilton, 1997).

1.1.3. Development of PET imaging for Medical Applications

The concept of PET for medical applications was first introduced in the early 1950s for studying localizations of brain tumors (Wrenn et al., 1951). PET has been known for its superior sensitivity compared to other imaging modalities, however, the radiation event data detected by PET cameras has to be algorithmically reconstructed to produce three-dimensional distributions of radioactivity which has been particularly challenging owing to a high noise-to-signal ratio. Thus, the collection of information takes time and a low anatomical resolution is usually resulted (Bendriem et al, 1998).

To produce a better image, a second scan with an anatomical technique like computed tomography (CT) or magnetic resonance imaging (MRI) was used. A method that combines the imaging data obtained from the first PET scan and a second scan (CT or MRI) was used to produce a better image. In the late 1980s, this method was successfully achieved for brain cancer detection (Pelizzari et al., 1989; Woods et al., 1993). This technique works for non-moving organs such as the brain. However, image alignment of other parts of the body (especially the heart and lungs) was problematic

due to patient movement. In 1994, the design of a PET/CT system, which combined a PET scanner and a CT scanner into one unit, was first introduced (Townsend, 2008). The system comprised a PET scanner and a CT scanner situated next to each other. Since the two scans can be performed consecutively during the same session, with the patient not changing position between the two types of scans, the two sets of scan images are more precisely co-registered. In this way, the areas of abnormality on the PET imaging can be better correlated with the anatomical information obtained on the CT images. This combined scan method is very useful in showing detailed views of organs or structures with high anatomical variations, most commonly observed in moving human organs (e.g. heart), but not so much with the brain. An example of a PET/CT scan showing a clearer image of body organs with high radioactivity uptake is shown in Figure 1.3.

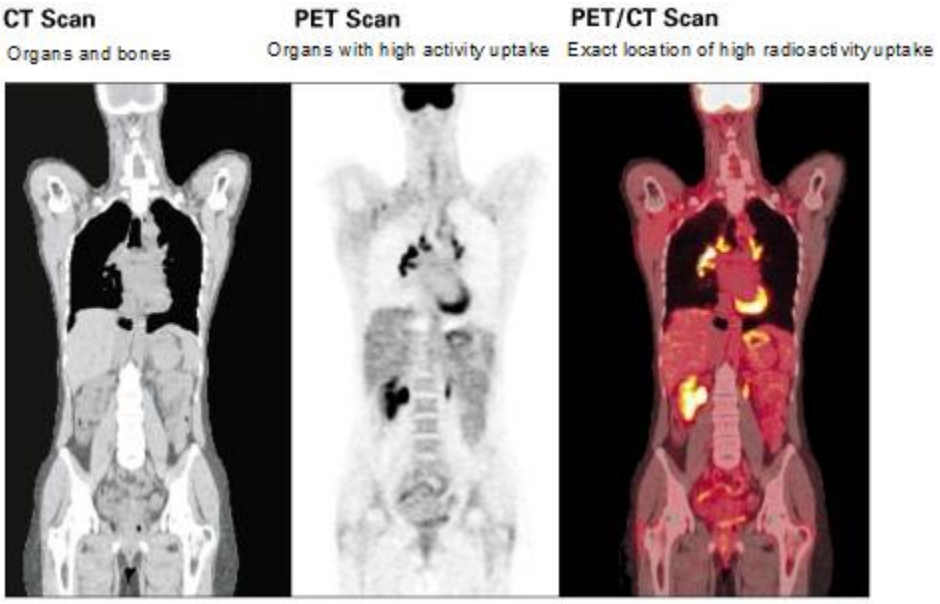

Figure 1.3 Comparison of scanned images obtained using CT scanner and PET scanner and a PET/CT Scanner.
Obtained from http://www.upmc.com/patients-visitors/education/tests/pages/petct-scan.aspx

In 2001, the first commercial PET/CT scanner was introduced (Burger et al., 2002). Since then, the PET scanners used were combined PET/CT systems. To date, the PET/CT scanners carry the reputation as a state-of-the-art functional imaging technique which depicts the spatial distribution of metabolic or biochemical activities in

the human body as well as anatomical imaging information. PET imaging has the unique potential to study non-invasively the physiological and biochemical processes taking place in healthy and diseased subjects. This imaging technique is considered particularly valuable in the field of oncology, where the location of cancerous tissues can be revealed to guide surgical resection (Brink, 2005).

While researchers know the value of PET for diagnosing and staging cancer, the future of PET imaging is for monitoring cancer therapy. Researchers have increasingly explored the use of PET as a tool for investigating the treatment outcome of using new therapeutic drugs (Miller et al., 2008). For drugs to work in clinical trials, it is important that the pharmacokinetics is fully understood. PET/CT has a unique possibility to investigate the pharmacokinetic effects of drug candidates. The imaging technique can be used to predict the efficacy of investigational lead drug candidates at low dosages *in vivo* through "microdosing" studies. With microdosing, a reduced safety requirement could be claimed for clinical studies since the mass of the injectable drug is so low (but still detectable) that it will not provoke any toxic or biochemical effects to the patients (Bergstrom et al., 2003).

1.2. PET Radionuclides

1.2.1. Radionuclide Production by Cyclotron

PET scan requires the use of positron-emitting radionuclides. Short-lived radionuclides can be produced in a cyclotron by bombarding stable nuclides with charged particles to initiate nuclear reactions such as bombardment of ^{18}O nuclide by protons [i.e.^{18}O (p,n) ^{18}F], see Scheme 1.5.

$$^{18}O + p \rightarrow {}^{18}F + n$$

Scheme 1.5 Proton bombardment of ^{18}O to produce radioactive ^{18}F

A cyclotron is a particle accelerator whose basic operation involves the acceleration of charged particles or ions by their attraction to or repulsion from charged electrodes (Figure 1.4A). In a negative ion cyclotron, charged (e.g. H^-) ions are produced

in an ion source (*S*) that is located within the gap in a cyclotron. Then, these ions are attracted towards the oppositely charged hollow structures called dees (*A* and *B*). The dees are kept in a high vacuum tank and an electromagnetic field is applied between them. The magnetic field in the dees induces a circular path for H^- ions during their acceleration. Since a radiofrequency alternating voltage is applied between the dees, the charged particles are accelerated as they cross the gap between the dees (like charges repel and unlike charges attract) and they move in a bigger radius. Eventually, the high energy particles are extracted by passing through the deflector (*D*). The deflector which contains the extraction foil, usually made of graphite, then strips off the electrons and reverses the charge of the ion from negative to positive (e.g from H^- to H^+). Since the magnetic field is continually applied, reversing the charge causes the proton (H^+) to be deflected in the opposite direction, out of the cyclotron, and an H^+ beam of defined energy is formed. A beam port (*W*) is located where the H^+ ions or protons pass out of the cyclotron. The H^+ beam enters a target body through a vacuum isolation foil, helium cooling outlet, and target isolation foil (usually Havar). The target body holds the target material (e.g. $^{18}O_2$ or $^{14}N_2$), as shown in Figure 1.4B. For instance, this extracted H^+ beam is used to irradiate targets of stable elements (e.g. $^{18}O_2$ or $^{14}N_2$) and nuclear reactions take place as in scheme 1.5.

The target material for the irradiation must be pure and preferably monoisotopic or at least enriched isotopically to avoid contamination by extraneous radionuclides. In most cases, appropriate chemical methods, such as solvent extraction, precipitation, ion exchange and distillation, are required to separate the target material from the radioisotopes produced (e.g. ^{18}F).

The cyclotron process can be used to accelerate protons, neutrons, deuterons, α particles and hydride ions. These high-energy particles will be used to irradiate targets to produce radionuclides. Cyclotron-produced radionuclides are usually rich in protons in the nuclei and therefore they decay by β^+-emission and/or electron capture (Saha, 2006).

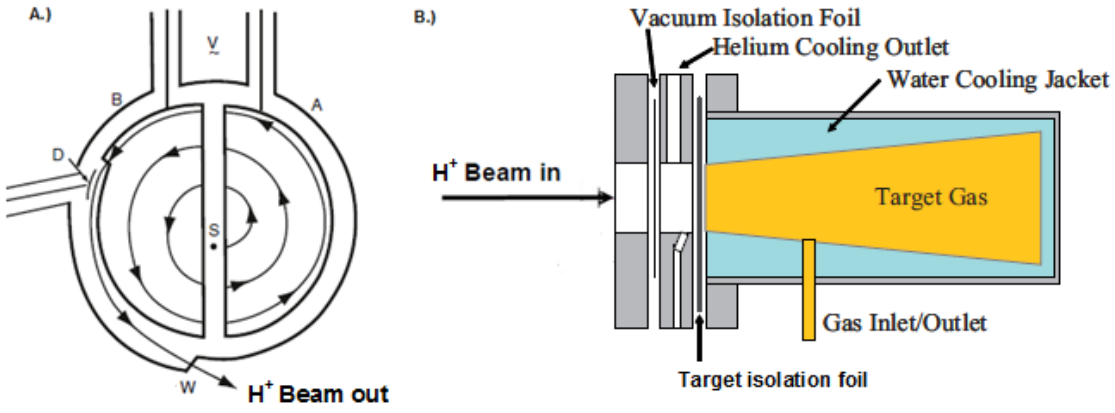

Figure 1.4 Schematic of a typical cyclotron
Note: A) Charged electrodes *A* and *B* are dees under vacuum, *S* ion source, *D* is deflector, *V* is alternating electrical voltage, *W* is window or beam extractor (with permission from Saha, 2006) B) Schematic of a typical cyclotron target body used for gaseous target materials, e.g. O_2 (as shown in IAEA, 2009).

The typical energy of medical cyclotrons ranges between 3-19 MeV (Saha, 2006). Small cyclotrons are compact negative ion (H^-) cyclotrons that are commonly used for production of short-lived radionuclides (e.g. ^{18}F, ^{11}C, ^{13}N, ^{15}O) using H^+ beam with lower energy (e.g. 4-14 MeV for ^{18}F, 7-15 MeV for ^{11}C, etc.). In contrast, several medically-useful radionuclides require H^+ beam with higher energy such as ^{111}In (6-40 MeV), ^{67}Ga (20-30 MeV), etc. and so large cyclotrons are used for the production of these radionuclides.

1.2.2. Characteristics of PET Radionuclides

There are several important characteristics that should be considered for isotopes to be used in PET imaging. First, it is the isotope half-life ($t_{1/2}$) which should be short enough for the isotope to decay rapidly in the human body to give the least radiation dose incurred by the patient. But the half-life should be long enough to allow for synthesis of the radiopharmaceutical in sufficient amounts and for it to be manufactured commercially at offsite locations before being shipped to PET imaging centers. Furthermore, the $t_{1/2}$ of the radioisotope must be compatible with the biological clearance half-life of the tracer and of the biochemical process being studied.

Second, it is also important that positrons should have relatively low energy and therefore travel in short ranges in biological tissues. The range is defined as the distance which the positron travels before annihilating with a nearby electron. The precise annihilation point is usually a few hundred μm from the actual decay location. . If positron annihilation and gamma emission does not occur in close proximity to the location of the radionuclides, there is an error in location which will ultimately contribute to a "blurred PET image (Williams et al., 2005). Therefore, isotopes with lower positron energy tend to produce images of better spatial resolution.

Third, as discussed in Section 1.1.1, cyclotron-produced radionuclides can decay by β^+-emission or electron capture, radionuclides that favor positron emission over electron capture yield high positron abundance. The higher the number of positrons, the better the quality of the image produced. On the other hand, electron capture does not contribute to producing the image but only produces extra radiation dose to the patient. The higher the radiation dose, the higher is the probability of harmful effects to the patient.

Lastly, it is also important to consider the availability and purity of the targets for the production of PET isotopes. The targets should be inexpensive and readily available. It is also ideal that the nuclear reaction between the H^+ beam and the target can occur in an efficient and clean manner and so extensive isotopic purification can be minimized or avoided. For example, the most commonly used target to produce ^{11}C is $^{14}N_2$ gas, and $H_2{}^{18}O$ or O_2 gas are the targets for ^{18}F production since these target materials are readily available.

1.2.3. Traditional and Non-traditional PET radionuclides

There is a wide variety of different β^+-emitting isotopes utilized in PET and the most common isotopes used in nuclear medicine are summarized in Table 1.1. The radionuclides ^{11}C, ^{13}N and ^{15}O, typically categorized as "traditional PET radionuclides", are isotope of elements commonly found in nature and can be used to create PET tracers that are indistinguishable from their non-radioactive counterparts. The use of these three radionuclides is of great advantage if the cellular target (e.g. receptor, cell

surface protein) of interest is sensitive to the difference in the molecular structure of the labeled compounds. However, the short half-life of these three isotopes often limits their use (Welch and Redvanly, 2003). For instance, owing to its short half-life, ^{11}C is available for labeling only to those radiochemistry laboratories with a cyclotron located on-site.

The isotope ^{18}F is not a natural constituent of biomolecules and thus, it is not technically considered as a traditional PET radionuclide. ^{18}F however, is an important PET isotope since it can substitute atoms (such as H and OH) in a biomolecule or ^{18}F can be placed in a position where its presence does not significantly alter the biological behavior of the biomolecule (Welch and Redvanly, 2003). Furthermore, ^{18}F has desirable properties ideal for PET imaging, as discussed in the next section (1.2.4).

Table 1.1 Common positron-emitters used in PET

Radionuclide	Half-life (min)	Decay Mode	Maximum Positron Energy (MeV)	Decay product
^{11}C	20.4	100 % β^+	0.96	^{11}B
^{13}N	10.0	100 % β^+	1.19	^{13}C
^{15}O	2.07	100 % β^+	1.723	^{15}N
^{18}F	109.8	97% β^+, 3% EC	0.635	^{18}O
^{64}Cu	768	17.9% β^+, 37.1% β^-, 45% EC	0.656	^{64}Ni
^{68}Ga	67.6	90 % β^+, 10 % EC	1.899	^{68}Zn

Note: Adapted from Welch and Redvanly, 2003. EC= electron capture, β^+=positron emission, β^-= electron emission.

With the advent of a number of new biomarkers, there has been an increased use of new isotopes (other than ^{11}C, ^{13}N, ^{18}O and ^{18}F) to create a novel approach in developing new PET imaging probes. For instance, the use of radiometals in PET chemistry has emerged. While a radiometal can be tightly bonded to a chelator, the latter can be covalently linked to a biologically active molecule. The use of this type of radiotracer in PET is attractive since molecules with large molecular weights (e.g. peptides and proteins) can tolerate chelator modifications and still retain the molecules' ability to bind to a cellular target of interest. Some examples of radiometals that can be used for PET imaging are ^{68}Ga, ^{64}Cu, ^{86}Y, ^{89}Zr and ^{44}Sc. For therapy applications, ^{90}Y

(β), ^{225}Ac (α) and ^{212}Pb (β^-) are used with antibodies (immunoconjugates) or peptides (Price et al, 2014).

Each radiometal ion has unique chemical properties, and the choice of the radiometal depends on the type of chelators and/or the type of cellular targets being studied. For example, ^{64}Cu is often chosen since this positron-emitter has short range in biological tissues, and with a longer half-life which allows transport of radiometal for labeling to locations without cyclotron. Recently, scientists were able to develop a good chelator for ^{64}Cu which is called the 'diaminosarcophagine' chelator. The use of this chelator has permitted the synthesis of stable ^{64}Cu-labeled peptides (Ma et al., 2009) and antibodies (Voss et al., 2007).

1.2.4. Fluorine-18

^{18}F is one of the most commonly used isotopes for PET imaging due to its appropriate decay half-life of 109.7 min (i.e. short enough to decay rapidly in the human body for pharmacokinetic clearance but long enough to allow time for synthesis of radiotracers), and also to be manufactured commercially at offsite locations then shipped to PET imaging centers. ^{18}F also has desirable radionuclide properties such as low positron energy (see Table 1.1), high positron abundance (approx. 97 % β^+-emission), high availability of enriched target material (such as $H_2{}^{18}O$), and giving high purity product (Welch and Redvanly, 2003).

There are two reaction pathways for the production of ^{18}F that are commonly used today. The first pathway is via proton irradiation of ^{18}O-enriched oxygen gas target to produce $[^{18}F]F_2$ as shown in Scheme 1.6. The $[^{18}O]O_2$ gas target is loaded in a nickel target body. Afterwards, $[^{18}O]O_2$ is irradiated with protons followed by cryogenic recovery of the O_2 target material. However, this method leaves most of the $[^{18}F]F_2$ attached to the target walls. Since $[^{18}F]F_2$, cannot be efficiently purged from the walls, the addition of $^{19}F_2$ carrier to the target body is necessary, followed by re-irradiation with protons in the presence of a noble gas such as Kr. Approximately 60 % of the radioactivity is recovered with only 30 μmol of $^{19}F_2$. Since $^{19}F_2$ carrier is added, a lower specific activity (SA = 0.35-

0.6 GBq/μmol) results. The ^{18}F produced by this method is called “carrier-added” due to the presence of non-radioactive ^{19}F (Hess et al., 2000).

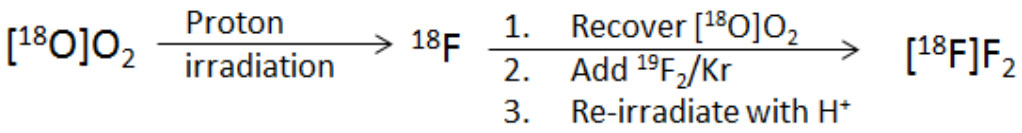

Scheme 1.6 Production of Carrier-Added $[^{18}F]F_2$ via proton irradiation of $[^{18}O]O_2$

The second pathway of ^{18}F production is via proton irradiation of ^{18}O-enriched water target as illustrated in Scheme 1.7. Using this approach, less than 1 mL of ^{18}O-enriched water is used and the $[^{18}F]F^-$ can be collected and used in a ‘no-carrier-added’ fashion. Target wall materials containing Ni, Ti and Ag are acceptable but Cr, Fe or Co are undesirable as they possibly produce insoluble $[^{18}F]$-metal fluorides. Since ^{18}O-enriched water is expensive, it is usually recovered for re-use after removal of the $[^{18}F]$fluoride by, for example, its adsorption on an anion exchange column.

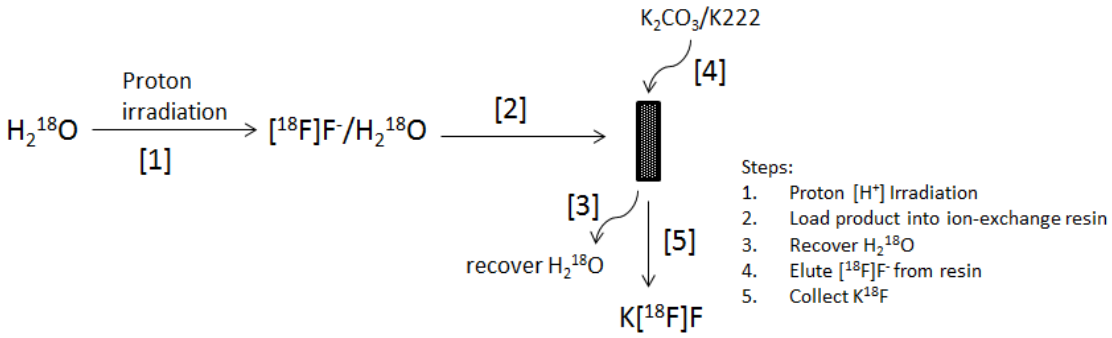

Scheme 1.7 Production of No-Carrier-Added $[^{18}F]F^-$ via proton irradiation of $H_2{}^{18}O$

The use of ^{18}O-enriched water as a target for proton irradiation is intrinsically high-yielding. The theoretical maximum specific activity (SA), which should be achieved with a carrier-free $^{18}F^-$, is 63,000 GBq/μmol (Mason et al., 2005). The specific activity of carrier-free $^{18}F^-$ is calculated using the half-life and the molar mass of the radionuclide (Saha, 2006). However, this theoretical value is impossible due to the pervasiveness of fluorine in the cyclotron components and subsequent chemical equipment which leach ^{19}F into the $[^{18}F]F^-$ product collected. Because of the presence of contaminating ^{19}F, most

sites produce [^{18}F]F$^-$ with SAs in the range of 300-600 GBq/μmol (Ross et al., 2011). Since higher radioactivity yields and higher SAs are achieved by using the no-carrier-added method, this process is usually preferred over the carrier-added method for production of ^{18}F.

1.3. ^{18}F Radiopharmaceuticals

1.3.1. [^{18}F]fluorine Chemistry

PET imaging requires positron-emitting biomolecules which selectively binds to the biological tissue of interest (i.e. cellular targets or receptors). These positron-emitting biomolecules are called radiopharmaceuticals and they are meant to be introduced into the human body for diagnostic purposes. As an example, radiopharmaceuticals can be used to measure the *in vivo* activity of biomolecules by following the rate of disappearance of a labeled substrate or the rate of appearance of a labeled product, leading to non-invasive visualization of the disease state. To trace such *in vivo* processes, the biomolecule has to be labeled with a positron-emitting radionuclide, such as ^{18}F.

^{18}F is an ideal radioisotope for PET, and biomolecules are labeled with ^{18}F to form aryl and heteroatomic functionalities containing a C-F bond. Carbon-fluorine bond formation for the production of ^{18}F radiopharmaceuticals is generally achieved by either electrophilic or nucleophilic substitution. There are also two commonly used ^{18}F-labeling strategies. One is the direct incorporation of ^{18}F to a biomolecule and the other is the indirect labeling of ^{18}F via prosthetic groups.

First, electrophilic substitution proceeds with labeling a radiotracer compound by using [^{18}F]F_2 which is produced via proton irradiation of ^{18}O-enriched O_2, as previously discussed (see section 1.2.4). An example of electrophilic substitution reaction is the synthesis of [^{18}F]fluoroDOPA (Scheme 1.8), a radiopharmaceutical used to assess the extent of dopamine synthesis and metabolism in presynaptic nerve terminals (Namavari et al., 1992). However, this substitution reaction results in radiotracers of low specific activities or high presence of non-radioactive counterparts at micromolar quantities.

Thus, electrophilic substitution is limited to the preparation of relatively non-toxic compounds in which their binding is not affected by non-radioactive fluoroDOPA. Because of these limitations, electrophilic substitution is less preferred in the synthesis of ^{18}F-labeled radiotracers.

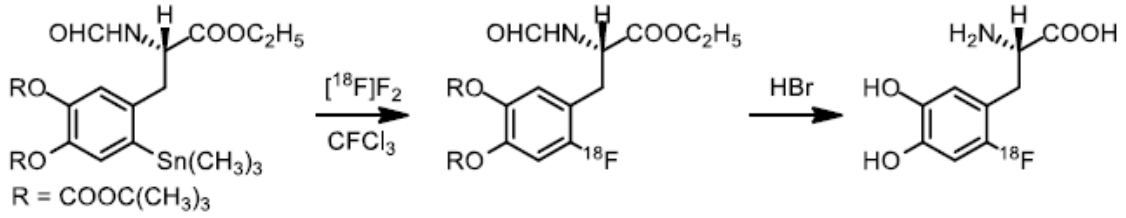

Scheme 1.8 Synthesis of [^{18}F]fluoroDOPA via electrophilic substitution reaction using [^{18}F]F_2 (Namavari et al., 1992)

Second, in nucleophilic substitution, the [^{18}F]fluoride ion is used as a nucleophile for synthesizing PET radiotracers. A good example of this substitution reaction is the Balz-Schiemann reaction (Scheme 1.9) wherein ^{18}F replaces ^{19}F in the tetrafluoroboronic acid. This reaction is used to synthesize ^{18}F-labelled radiotracers such as L-phenylalanine, L-tryptophan and L-DOPA (Laali et al., 2001).

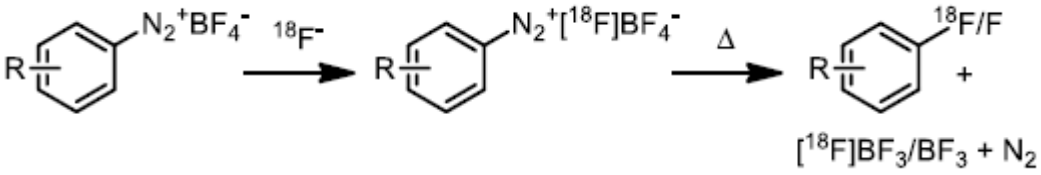

Scheme 1.9 The Balz-Schiemann reaction using [^{18}F]fluoride as the nucleophile (Laali et al., 2001)

Nucleophilic substitutions that involve [^{18}F]fluoride anion start with a drying step to remove water. It is because fluoride is heavily solvated in water due to strong hydrogen bonding and therefore the anion is less reactive as a nucleophile (Clark, 1980; Vlasov, 1993). Therefore, prior to synthesis, the first step is to remove the bulk [^{18}O]water by passing the irradiated $H_2{}^{18}O$ target water through an ion exchange resin column. The [^{18}F]fluoride is adsorbed onto the resin while $H_2{}^{18}O$ water flows through (Schlyer et al., 1990). This procedure will first recover the expensive [^{18}O]water which may be reused after purification (Asti et al., 2007; Moon et al., 2007). Then, the

adsorbed [^{18}F]fluoride is eluted off the resin using an eluent that normally contains an aqueous solution containing an inorganic anion (K_2CO_3, $KHCO_3$) and a phase transfer agent such as cryptand (e.g. like aminopolyether, Kryptofix™ (K222) or tetrabutyl ammonium) dissolved in acetonitrile (Hamacher et al., 1986; Brodack et al., 1988).

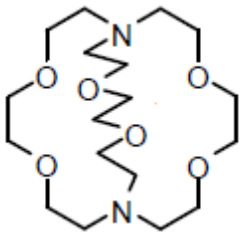

Figure 1.5 Structure of aminopolyether Kryptofix 2.2.2 cryptand (K2.2.2.)

The eluted [^{18}F]fluoride is complexed by the phase transfer agent and the solution is then evaporated to dryness by heating it under reduced pressure. Aliquots of pure acetonitrile are added mainly because of its suitability to form an azeotropic acetonitrile-water mixture which facilitates the drying step (Gillies et al., 2006). The drying vial is then heated at about 90-95 °C under a constant flow of inert gas (e.g. helium or argon) at reduced pressure and the vial is stirred by a rod or shaken to help the evaporation of the (water/acetonitrile) azeotrope. Since a small amount of water stays in the vial another portion of acetonitrile is added and the drying step continues. After the second drying step (another 2–3 min) a dry [^{18}F]fluoride-K222 complex is produced. Some researchers will add a third step to ensure complete drying of the [^{18}F]fluoride-K222 complex, which is used in the subsequent synthetic step. In the case of automated synthesis, the risk of contamination and human errors are greatly reduced in the drying procedure making it a reasonable approach in producing [^{18}F]fluoride (Wester et al., 2011).

For synthesis, the dried residue of the [^{18}F]fluoride-K222 complex is first dissolved in a polar aprotic solvent. A suitable amount of precursor is added and then the mixture is heated to facilitate the synthetic reaction (Hamacher et al., 1986). Acetonitrile, in contrast to other solvents such as DMSO or DMF, has the advantage that it can easily be removed by evaporation. The choice of solvent is also dictated by the nature of the precursors or by the reaction temperature.

Direct labeling involves the direct incorporation of [^{18}F]fluoride to a biomolecule via substitution reaction (Graham et al., 2014; Huang et al., 2014; Tredwell et al., 2014). For example, [^{18}F]fluoride substitution of the hydroxyl group at the 2' position in glucose (see Figure 1.5) produces 2-[^{18}F]fluoro-D-glucose ([^{18}F]FDG), which is a clinically-approved ^{18}F radiopharmaceutical. In 1980s, [^{18}F]FDG was found to accumulate in tumours, thus paving the way to the evolution of PET as a major clinical tool in cancer diagnosis (Som et al., 1980). [^{18}F]FDG mimics glucose in that it is susceptible to phosphorylation at the 6' position by hexokinase to form glucose-6-phosphate (G6P). Unlike G6P, the generated 2-fluoro-glucose-6-phosphate resists further enzymatic transformation by phophohexose isomerase and so it becomes entrapped intracellularly. As a result, the distribution of [^{18}F]FDG is a measure of metabolic activity of glucose in the body. As many cancers exhibit elevated metabolic rates due to the increased levels of cell proliferation, [^{18}F]FDG has become an important marker for diagnosis of cancer and assessment of cancer progression. The general nature in the action of FDG in proliferating cancer cells allows the visualization of tumor in a variety of cancer types by PET imaging.

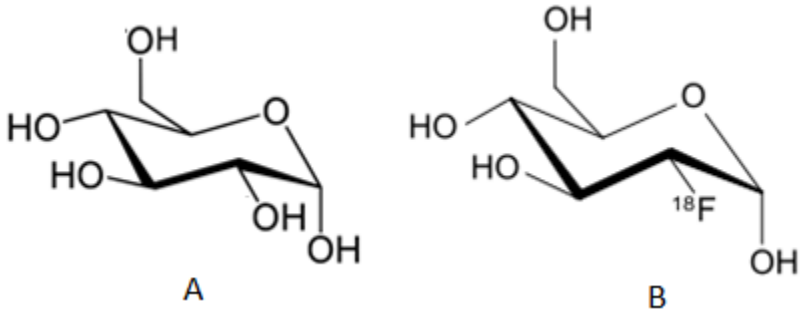

Figure 1.6 (A) structure of glucose molecule (B) 2-(^{18}F)fluoro-D-glucose, a glucose analog, with the positron-emitting radioactive isotope [^{18}F]fluorine

Direct ^{18}F-labeling is usually only compatible with small biomolecules since labelling conditions requires scrupulously dry conditions, achievable often at elevated temperatures. These conditions are not compatible to most large biomolecules which are heat-sensitive. To address this problem, an indirect labeling strategy has been developed wherein an ^{18}F-containing small molecule called a prosthetic group is first synthesized and then used for labeling large molecules (Thumshirn, G., 2003; Welch

and Redvanly, 2003). This indirect labelling strategy is typically used for the labeling of macromolecular biological targeting agents such as peptides, proteins and oligonucleotides.

One disadvantage of conventional ^{18}F-labeling (based on C-F bond formation) is the heating required (after pre-concentration step) to significantly reduce the amount of water. However, most fluorination reactions require the complete removal of water in the reaction mixture. The time required to perform this drying step increases the overall synthesis time, leading to less ^{18}F resulted due to radioactive decay. Another disadvantage is the need of a phase transfer agent added to enhance the solubility and nucleophilicity of [^{18}F]fluoride in organic solvents. The aminopolyether Kryptofix 2.2.2 cryptand (K2.2.2) is usually considered as an ideal phase transfer agent to enhance the synthetic reaction (Coenen et al., 2007). However, the cryptand is toxic [LD50 (rat) = 35(±2) mg/kg (i.v.)] (Baudot et al., 1977) and must be completely removed from product mixture prior to *in vivo* use of the radiotracer.

Furthermore, direct C-F [^{18}F]fluorination of large biomolecules (such as proteins and peptides) is undesirable since the reaction requires elevated temperatures (80–150^{o}C), often resulting in decomposition of the precursor and/or the product. Thus, aqueous [^{18}F]fluoride chemistry (*vide infra*) have been developed whereby prosthetic groups, which are small molecules that can be prepared in aqueous conditions, are synthesized first, and then they are attached to a biomolecule in a second reaction. (Ting et al., 2008)

1.3.2. Aqueous [^{18}F]fluoride chemistry

The difficulties encountered in conventional synthesis of ^{18}F radiotracers have led to the exploration of other methodologies which do not require C-F bond formation. Ideally, a large biomolecular imaging agent could be synthesized as a stable precursor that could be rapidly labeled in a single, high-yielding step under aqueous conditions via attachment of a prosthetic group which is labeled with ^{18}F.

It has previously been reported that di-tert-butyl(p-benzaldehyde)-silyl-[^{19}F]-fluoride (SiFA-A) would undergo isotopic exchange with [^{18}F]fluoride (Scheme 1.10)

under mild conditions (Schirrmacher et al., 2007). The authors were able to demonstrate that this small molecule can be used as a starting compound for labeling different ^{18}F-labeled peptides, and the labeled peptides are stable *in vivo*. The RCY of the labeled compound reported was >75 % and the specific activity was 225-680 GBq/µmol (6.08–18.4 Ci/µmol) before HPLC purification.

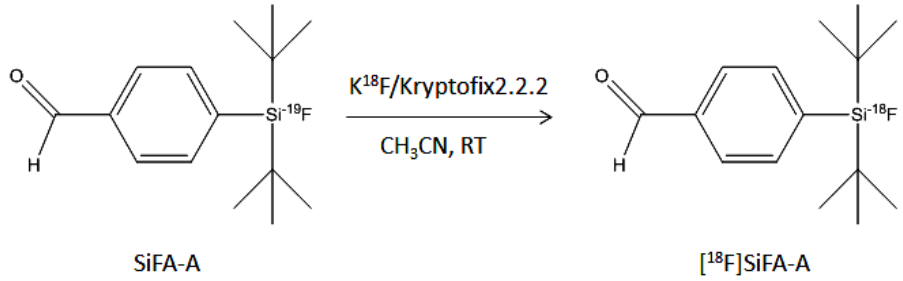

Scheme 1.10 Reaction of nonradioactive SiFA-A with [^{18}F]fluoride to form [^{18}F]SiFA-A

Reactions of [^{18}F]F$^-$ with boronic esters to form aryltri-[^{18}F]fluoroborates via ^{19}F-^{18}F isotope exchange (Scheme1.11) have been developed by the group of Perrin (Liu et al., 2012). The product, ArB[^{18}F][^{19}F]$_2^-$ was synthesized through a rapid, single step, aqueous ^{18}F-labeling method that proceeds under mild conditions. RCY value of 50 % and specific activity of nearly 555 GBq/µmol (15 Ci/µmol) were achieved when initial activity of >800 mCi was used. However, when lower initial activities, i.e. 400 mCi, were used, lower specific activities of approximately 111 GBq/µmol were obtained.

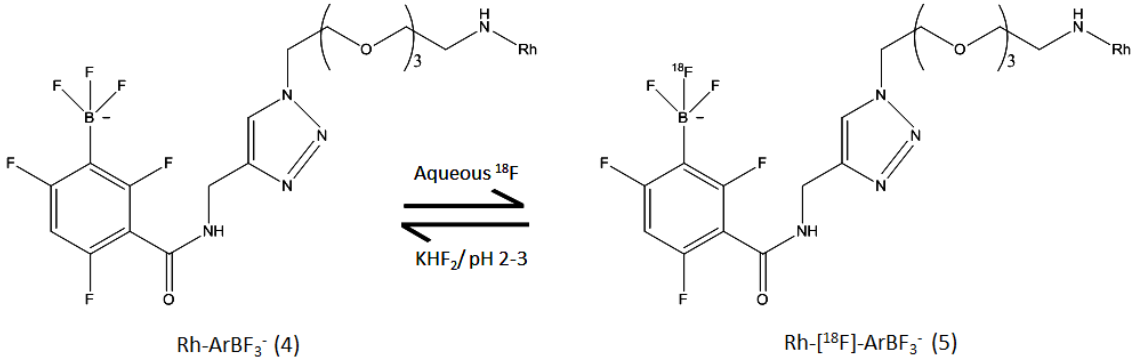

Scheme 1.11 Rhodamine-^{19}F-ArBF$_3$ (4) precursor undergoes isotope exchange with aqueous [^{18}F]F$^-$ to form rhodamine-^{18}F-ArBF$_3$ (5)

Al-F chemistry (Scheme 1.12) was also reported as an aqueous labeling method based on the chelation of [^{18}F]-aluminum fluoride (Al^{18}F) by 1,4,7-triazacyclononane-1,4,7-triacetic acid (NOTA) (Laverman et al., 2010). The ^{18}F-labeled NOTA-octreotide has been proven to be stable *in vitro* and *in vivo* and it effectively binds to cell targets to image tumor sites. The RCY reported was 50 % after the labeled product was purified by HPLC to remove unbound Al^{18}F and unlabeled peptide. The overall synthesis time was reported to be 45 min. at 100 ^{o}C. The specific activity was 45 GBq/µmol.

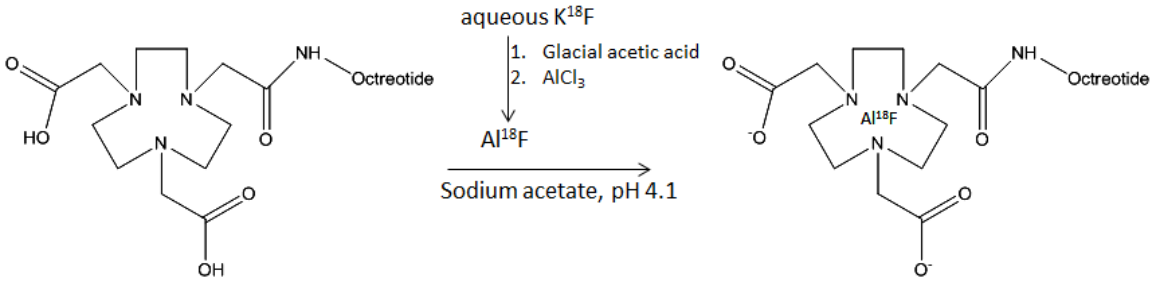

Scheme 1.12 Preparation of Al[^{18}F] and chelation with NOTA-octreotide

Finally, S-F bond formation (Scheme 1.13) was achieved by using arylsulfonyl chloride derivatives to capture [^{18}F]F^{-} (Inkster et al., 2012). The reaction was conducted using aqueous conditions at room temperature for 10-15 minutes. The ^{18}F-labeled prosthetic compounds produced have radiochemical purities as high as 96%, with specific activities of around 105 GBq/µmol. The prosthetic group was further coupled to a peptide such as bombesin (BBN-OX-MESIT-SO_2[^{18}F]F) and gave an RCY of 56%. However, it is found that the peptide was not stable in mouse serum for more than 15 minutes (Inkster et al., 2012). In a study published by Matestic et al. (2013), another ^{18}F-labeled sulfonyl fluoride derivative, 2,4,6-triisopropylbenzenesulfonyl [^{18}F]fluoride, exhibited excellent stability in rat plasma at 37 °C for 2 hours.

In recognizing a need for improved indirect ^{18}F-labeling for sensitive targeting agents or biomolecules, all of the above reported novel fluoride chemistry sheds light on the need for developing a high-yielding and water-compatible radiolabeling procedure for producing PET radiotracers. Herein, we apply a novel platform, called magnetic droplet microfluidics (MDM) technology, for aqueous-based S-F and B-F radiofluorination.

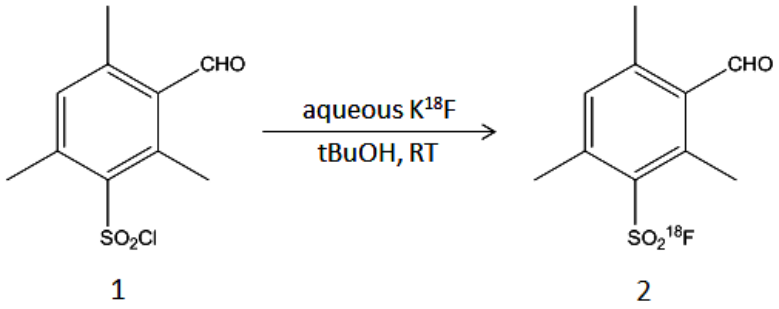

Scheme 1.13 Conversion of non-radioactive 3-formyl-2,4,6-trimethylbenzenesulfonyl chloride (1) to 3-formyl-2,4,6-trimethylbenzenesulfonyl [^{18}F]fluoride (2)

1.4. Automation of the production of [^{18}F]-labeled radiotracers

PET chemistry requires positron-emitting nuclides with activities that typically range from millicurie to curie levels and this amount of activity is too high for hands-on manipulation (Svadberg, 2012). The short half-lives of radioisotopes also necessitates on-demand production of many experimental radiotracers, with each dose being produced separately just before use. Furthermore, it should be ensured that the synthesis and purification procedures pass the quality control criteria in order to meet the standards required for human use. To overcome these challenges, it can be clearly understood that automation is an important aspect in radiochemistry synthesis. Ideally, all the steps required for radiosynthesis should take place inside a shielded hot cell with little or no human intervention to avoid high radiation exposure. Moreover, the increased need for radiopharmaceuticals in the preclinical setting clearly demonstrates the need for automated methods for an increased throughput of radiotracer production.

1.4.1. Vessel-based modular systems

During the advent of radiopharmaceutical development, automated, vessel-based systems have been developed for individual hot cells and for specific radiotracers (Barrio et al., 1981; Fowler et al., 1981). These systems had pre-programmed software and the operation could be controlled by a computer. Typically, the radiosynthesizers

were modular systems that included remote-controlled valves, solvent reservoirs, tubing and one or two reaction vessels. Since [^{18}F]FDG is the most important radiopharmaceutical used in oncology, this section will focus on discussing available vessel-based automated systems used for the synthesis of [^{18}F]FDG.

These automated systems can be subdivided into two categories (De Leonardis, 2012; Svadberg, 2012). The first category is the stationary systems where all connections of the tubings and valves are permanent and are not changed in daily operations. The reagents and precursors are manually loaded and these systems have vessels which can carry reagent volumes from 1 mL to 10 mL. These systems, however, are normally used only once per day because the levels of radiation after cleaning are still too high to allow reloading of the chemicals, cartridges, etc. in a safe manner. Examples under this category are the TRACERlab (GE Medical Systems) and Synchrom (Raytest, GmbH), see Figure 1.7 (De Leonardis et al., 2012).

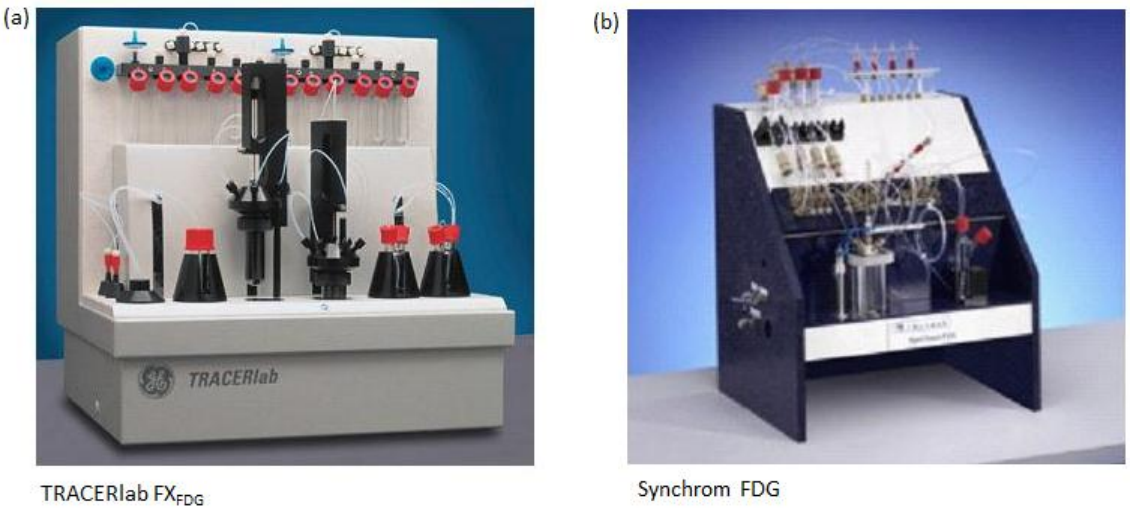

Figure 1.7 Stationary vessel-based modular systems: (a) TRACERlab Fx$_{FDG}$ (GE Medical Systems) (b) Synchrom FDG (Raytest, GmbH)

The second category is the cassette-type systems with disposable cassettes that can be replaced after each batch with no-cleaning procedure required. These systems avoid fluctuating results due to variable degree of cleaning between runs. However, one disadvantage is that the cassette cannot be remotely removed after synthesis due to radiation precautions. Examples under this category are the FASTlab (GE Healthcare

Technologies), Synthera (IBA Solutions) and Explora (Siemens Healthcare), see Figure 1.8.

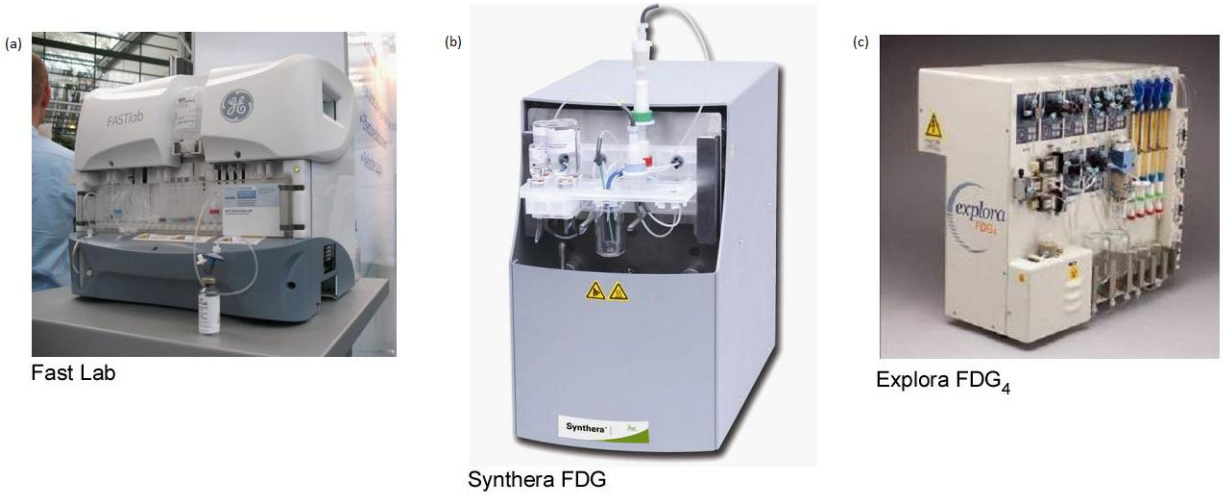

Figure 1.8 Cassette-type vessel-based modular systems: (a) FAST lab (GE Healthcare Technologies) (b) Synthera FDG (IBA Solutions) and (c) Explora FDG_4 (Siemens Healthcare)

1.4.2. Microfluidic Modular Systems

More recently, lab-on-a-chip devices have been explored as promising alternatives to traditional vessel-based radiotracer synthesis systems. These devices have superior control over reaction conditions, reduced reagent consumption and radioactive waste production, as well as the potential for automation with minimized shielding requirements. The RCY values are improved and purer products are produced due to the increased surface-area-to-volume ratio, enhanced mass and heat transfer and reduced diffusion distances achieved in the microchannels (Haroun et al., 2013; Wang et al., 2010).

The microfluidic device, which consists of a network of micrometer-sized channels, facilitates the manipulation of nanoliter to microliter amounts of volume where reagents are combined to react under specific experimental conditions. These miniaturized devices have been used in many biological and chemical applications ranging from micromixing, chemical synthesis, separation to chemical transformations (Wang et al., 2010; Wirth, 2008; Watts et al., 2007).

Although the use of microfluidic synthesizers for PET radiopharmaceuticals has shown promising results, these systems are currently predominantly applied to research and development applications. Utilization of this system for routine production of PET tracers for clinical use has been very limited until an acceptable level of reliability, repeatability, usability, and good manufacturing practice (GMP) compliance has been obtained (Rensch et al., 2013).

Currently, there are two major microfluidic systems available in the market, namely Advion Nanotek LF (Advion Biosciences, Inc., Ithaca, NY, USA) and Scintomics "μ-ICR" (Scintomics GmbH, Fuerstenfeldbruck, Germany) which will be described in detail in the following section.

1.4.2.1 Commercial modular microfluidic systems

In contrary to the vessel-based modular systems, the microfluidic modular system has integrated a microfluidic loop which can handle microliter volumes to carry out radiochemical reactions (Bouvet et al., 2010; Chun et al., 2010). These microreactor loops commonly have internal diameters of 10−300 μm and have much larger surface-to-volume ratio as compared to conventional vessel-type reactors.

Figure 1.9 (a) The microfluidic systems from Advion (Advion "Nanotek LF") which consists of a concentrator module, an evaporator module and a microreactor module (b) The microreactor module consisting of four microfluidic loops

Note: The loops are made up of coiled silica capillary (approximately 2 m in length with a diameter of 100-150 μm),housed in a brass ring sealed with a poly(silicone) connected to a heating system (Advion website, 2012; De Leonardis, 2012).

One commercially-available system is Advion NanoTek LF, see Figure 1.9. The system consists of a liquid flow reactor loop, an auxiliary pump module as well as a concentrator and evaporator module. The system also has an area for the independent heating of up to four microreactors. The microfluidic reactor loop, which consists of a coiled silica glass tube (100-150 µm × 2 m) with an internal volume of 15.7 µL, is housed in a brass ring sealed with poly(silicone) that is resistant to high temperature. The system features low reagent usage, allows fast synthesis, enables production of multiple radiotracers from a single [^{18}F]fluoride batch and the system can also be integrated with a purification module. The system gives the user the maximum flexibility for both research and clinical applications. (De Leonardis et al., 2011; Matestic et al., 2013)

Another commercial microfluidic system is Scintomics "µ-ICR" which is a compact platform for radiochemical reactions conducted in capillaries with an inner diameter of 250-500µm. This system contains several motorized syringes, high pressure injection valves, and a pump for automated injection, radioactivity detectors, heaters which are integrated into a compact reaction system (see Figure 1.10). This system is ideal for repetitive multidose and multitracer production. The advantages of µ-ICR are reduced reaction times, lower precursor amounts, decreased side product formation and improved yields.

Figure 1.10 The Scintomics "µ-ICR" (Scintomics)
Note: This system contains 2 multi-port motor syringes, 8 injection ports, 8 reagent valves, 2 T-mixers, 4 heaters, 4 integrated radioactivity sensors, 2 pressure regulators, 2 pressure sensors, 3 injection valves and 1 pump which can be connected to HPLC for automated injection. (Henriksen, 2008)

Both Advion NanoTek LF and Scintomics “µ-ICR” are examples of continuous-flow systems. They utilize simple hardware and incorporate conventional pumps and rotary motor valves, fluid connectors and capillaries in a single compact piece of equipment to make radiosynthesis more convenient. One disadvantage of continuous-flow microfluidics is the long flow paths used in the system and this increases the system pressure which may cause leakage in the tubing. Moreover, the long flow path results in high contact loss which lowers RCYs and. Another disadvantage is the high risk of channel clogging (Rensch et al., 2013).

1.4.2.2 Chip-based microfluidic system

In the chip-based system, conventional hardware are integrated with microfluidic techniques. This system typically comprises conventional components such as tubings, valves, syringe pumps as well as microfluidic devices such as monolithic devices or chip-like assemblies for turbulent mixing (Rensch et al., 2013).

A chip-based system (see Figure 1.11) has been used for clinical production of [^{18}F]fallypride, a neuroimaging radiopharmaceutical (Lebedev et. al, 2013). This paper was the first to report the production of a radiotracer in a microfluidic system to be used for human PET scan. In the system, the microfluidic technologies such as the fluoride pre-concentration system and a microfluidic batch reactor assembly were integrated with conventional hardware. ^{18}F solution was pre-concentrated to 45 µL and the released $^{18}F^-$ solution was delivered to a plastic reactor chip (5mm in diameter, 3mm deep and a total volume of 60 µL) which was produced via injection-molding. Nitrogen gas is used to push liquid flow through the entire system. The user can define the time, temperature and gas pressure. Operations can also be pre-programmed and can be linked together to achieve a fully automated system.

Another chip-based system is shown in Figure 1.12. The system is composed of a glass microfluidic device filled with recyclable anion exchange resin for the repeated recovery of [^{18}F]fluoride (De Leonardis et al, 2011). The device was tested for the trapping and release of [^{18}F]fluoride ions for over 20 experiments and 90-95% fluoride was recovered each time. The microfluidic chip was then connected to the Advion synthesis system (see Section 1.4.1) to perform a reaction with ethyl ditosylate (EtDT) to

produce [^{18}F]fluoroethyltosylate with 96 ± 3% yield (RCY). The overall time needed for conditioning, trapping, elution and regeneration was less than 6 min.

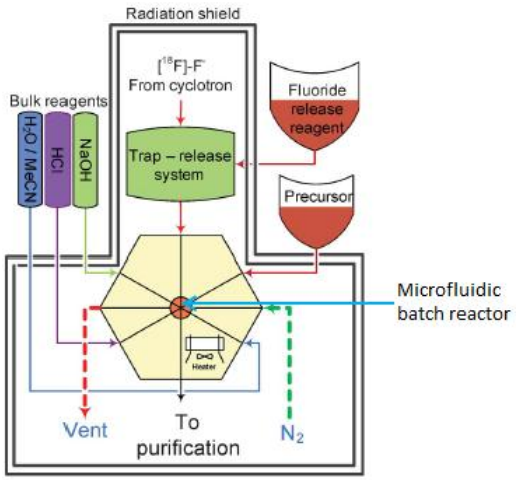

Figure 1.11 General scheme of the microfluidic system used for clinical production of [^{18}F]fallypride

Note: The microfluidic reactor with 8 valve ports is connected to a N_2 gas inlet, precursor delivery system, bulk reagent supply and fluoride trap-release system. The final product is transferred to a purification system (with permission from Lebedev et al., 2013).

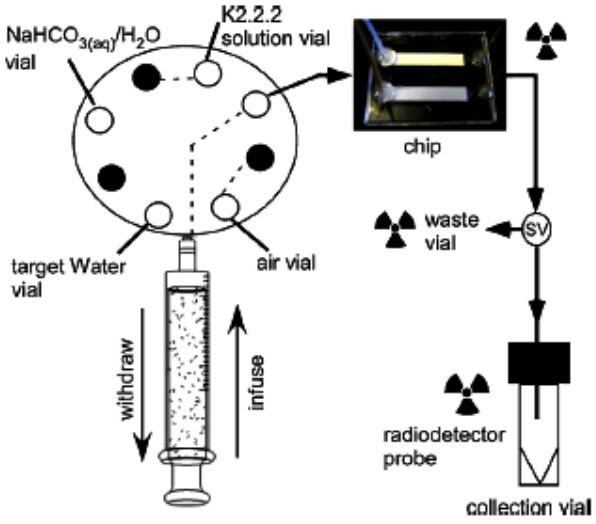

Figure 1.12 Schematic representation of the microfluidic chip for [^{18}F]fluoride pre-concentration

Note: A driving syringe was used to push different reagents onto the microfluidic chip. The chip outlet was connected to a solenoid valve (SV) which could direct liquid either to a collection vial or a waste vial. Radioactivity detectors were placed on the anion-exchange chip, next to the waste vial and next to the collection vial (with permission from De Leonardis et al., 2011).

The previously mentioned microfluidic system offers a promising method for automated production of ^{18}F radiotracers. However, there remains a need for developing alternative methods which are simpler, which minimizes the use of the number of loops and valves, and which uses cheaper set-up but can be easily automated. The high level of innovation is driven by the need for new technologies for producing functional elements and materials, as well as for developing new manufacturing processes.

1.4.2.3 Droplet microfluidics

Other than automation of liquid operations by vessel-based or chip-based microfluidic systems, automation could also be performed by manipulating liquid droplets in an open format. The manipulation of liquid droplets for sampling and reaction has been carried out by droplet microfluidics based on electrowetting (Day et al., 2012; Lee and Kim, 1998). Another method is to use a magnetic field to move magnetic particles and the liquid droplet associated with the particles (Dorvee et al., 2004).

The success of liquid drop manipulation depends on the quality of magnetic particles. These particles are usually made up of iron oxide that forms the core and each particle is encapsulated by a protective material (e.g. silica or polystyrene). The surface of the coated particles is then functionalized with chemical moieties for chemical reactivity.

Magnetic particles are commercially available in different sizes and functions. Sources include Dynabeads (Invitrogen, Paisley, UK), Biomag (PerSeptive Biosystems, USA), Biosphere (Biosource International), MACS MicroBeads (Miltenyi Biotec GmbH, Bergisch Gladbach, Germany), Estapor (Prolabo, France), MagnaBind particles (Thermo Fisher Scientific Inc., Illinois, USA) and many more (Bruce et al, 2004). Magnetic particles with surface moieties such as carboxylates are available for chemical modifications, but moieties with specific functions such as ion-exchange groups are not usually available. Moreover, particles with surface modification are expensive. Therefore, we explored in-house synthesis for making our own magnetic particles.

Several reports have been published regarding the synthesis of magnetic particles that consists of magnetite or iron (II and III) oxide (Abu-Much et al, Makhluf et

al, Lee et al). Bruce et al. (2004) reported a different method of synthesizing silica-coated magnetite nanoparticles on a large scale (greater than 20 g batch size). Bruce et al. (2004) introduced two methods for the preparation of Fe_3O_4 particles with silica coating. However, the functionalization and use of these particles for a specific purpose has not yet been reported. The efficient modification of the particle surface with different functional groups or ion-exchange groups for them to be used for a specific purpose remains to be demonstrated. This thesis focuses on the use of droplet microfluidics which is based on magnetic force-induced movement for producing [^{18}F]-labelled compounds in an open format. The synthesis of magnetite-based magnetic particles, their functionalization to provide ion-exchanging groups, pre-concentration of [^{18}F]fluoride and reaction of [^{18}F]fluoride with precursor compound will be described in detail in Chapter 2.

1.5. Thesis Motivation and Objectives

1.5.1. Thesis Motivation

The production of ^{18}F-based radiopharmaceuticals via aqueous fluorination requires three major steps. The first step is the pre-concentration of [^{18}F]fluoride, which is produced by the proton bombardment of the target material which is heavy oxygen water, ($H_2{}^{18}O$), and the radionuclide is released from the cyclotron in the form of $^{18}F/H_2{}^{18}O$ solution. The pre-concentration step involves selectively isolating [^{18}F]fluoride from $H_2{}^{18}O$ to recover $H_2{}^{18}O$ and to concentrate the [^{18}F]fluoride solution to increase nucleophilicity of fluoride ions (Cai et al., 2008). Currently, $^{18}F/H_2{}^{18}O$ solution is concentrated by first passing it through a short plug of anion-exchange resin and then by eluting the [^{18}F]fluoride with a K_2CO_3 aqueous solution and in the presence of a phase transfer catalyst such as a cryptand, e.g. Kryptofix 2.2.2 (K2.2.2), or a large organic counterion, e.g. tetrabutyl ammonium bicarbonate (Hamacher et al., 1986). The second step is the fluorination reaction which involves attaching [^{18}F]fluoride to a prosthetic group for subsequent attachment to a peptide or other biomolecules for PET imaging. After the synthesis of the labeled compound, a purification step should be conducted to remove unreacted ^{18}F ions and other impurities from it. Sterilization is also performed so

that the product will be suitable for patient injection. Purification can be accomplished by solid phase extraction (SPE) or HPLC.

Due to the short half-life of ^{18}F (109.7 min), it is necessary to execute these three steps rapidly without loss of precision and efficiency. The conventional method available to execute these mentioned steps for ^{18}F radiopharmaceutical production are difficult to achieve in a short time scale (within one half-life of the radioisotope). Furthermore, since the amount of ^{18}F ions in the solution is small, the radioactivity can be greatly reduced when the sample is transferred from one vial to another. All these will result to low radiochemical yields (Cai et al., 2008).

It is also important to note that handling radioactive species requires these key steps to be performed with the lowest possible exposure to the operator. Thus, ^{18}F radiopharmaceutical production requires an automated process to reduce production time, reduce radiation exposure and also minimize transfer of reagents during radiotracer synthesis, to reduce sample transfer loss.

It has been suggested that microfluidic devices can bring multiple advantages for radiopharmaceutical development. These advantages include (1) the ability to handle small volumes, (2) the potential of thorough mixing of reagents due to high surface to volume ratio, (3) good control over reaction conditions, (4) automated and fast synthesis and (5) high recovery of radioactive product. Moreover, microfluidic devices are easy to automate which would minimize both reaction times and operator radiation exposure. Moreover, there is a potential of reducing the infrastructure demands on any given facility as well as saving the shielding cost to perform radiopharmaceutical synthesis (Cai et al., 2008; Lu et al., 2010). All these advantages will lead to the increase of production yields and reproducibility of results. Thus, in this study, a microfluidic design is proposed as a potential method for the synthesis of ^{18}F radiotracers which aims to integrate the pre-concentration and synthesis steps on the same platform.

1.5.2. Thesis Objective and Outline

We report a study that aims to demonstrate a microfluidic platform to conduct [^{18}F]fluoride pre-concentration and synthesis of ^{18}F-labeled compounds through manipulating liquid droplets of microliter scale in an open format. The platform is called magnetic droplet microfluidics (MDM) and uses magnetic particles for liquid droplet manipulation. A moving magnet is used to translate the magnetic particles which hold a small liquid droplet by surface tension. The movement of the particles acts to separate small droplets from the big liquid drop and drag the droplets on the platform. The particles also have the ion-exchange property that is capable of capturing and releasing fluoride ions (Scheme 2.4). These particles are used to pre-concentrate the [^{18}F]fluoride ion in $H_2{}^{18}O$ liquid droplet. [^{18}F]fluoride ions are then released, and are used to synthesize a prosthetic compound which is subsequently used to label a large biomolecule for PET imaging. The use of the MDM platform is advantageous because of the ability to automate the process, to reduce human intervention, to keep reaction volumes low and to reduce reaction times.

For the purpose of this study, we chose aqueous ^{18}F-labeling reactions (see sections 2.5 and 2.6) as an application of the MDM platform. This is because we wanted to avoid a dry-down step, and to be able to perform the ^{18}F pre-concentration step and the synthesis reaction step on the same platform.

For aqueous ^{18}F chemistries, a few strategies had been reported, namely (1) fluorination of aryltri[^{18}F]fluoroborates (Liu et al., 2012), 2.) isotope exchange to form triorgano[^{18}F]fluorosilanes (Schirrmacher et al., 2007), 3.) coordination to aluminum to produce Al-^{18}F complexes (Laverman et al., 2010), and 4.) reaction with arylsulfonyl chlorides to form arylsulfonyl [^{18}F]fluorides (Inkster et al., 2012). We started our work on the arylsulfonyl fluoride chemistry considering our experience with this reaction in TRIUMF. The reaction was also reported to give good results such as high radiochemical yields using mild reaction conditions. We demonstrated the synthesis of 3-formyl-2,4,6-trimethylbenzenesulfonyl [^{18}F]fluoride (2) (see Scheme 1.13 in Section 1.3.2) as a prosthetic compound which has also been used to attach to a peptide for PET imaging (Inkster et al., 2012).

For this study, the same prosthetic compound, 3-formyl-2,4,6-trimethylbenzenesulfonyl [^{18}F]fluoride (2) is synthesized on the MDM platform from the corresponding 3-formyl-2,4,6-trimethylbenzenesulfonyl chloride precursor (Scheme 1.13) on the MDM platform and the reaction yields were compared with those obtained using the conventional method. The MDM method is further validated by extending the application to another aqueous ^{18}F transformation such as the aryltrifluoroborate formation (Liu et al., 2012) by the synthesis of rhodamine-^{18}F-ArBF_3 (5) (see Scheme 1.11).

In this study, we have:

1. Tested a liquid manipulation method on the microfluidic platform called magnetic droplet microfluidics (MDM)

2. Synthesized magnetic (Fe_3O_4-based) particles. The particle surfaces had been modified to contain a quaternary methylammonium (QMA)-iodide, so that the particles had the ion-exchange property to capture and release [^{18}F]F^-.

3. Characterized the particles using Energy-Dispersive X-ray(EDX)

4. Optimized reaction conditions for good capture and release efficiency of QMA-modified magnetic particles

5. Concentrated $^{18}F/H_2{}^{18}O$ solution using the MDM platform

6. Pre-concentrated [^{18}F]fluoride and synthesized 3-formyl-2,4,6-trimethyl-benzenesulfonyl [^{18}F]fluoride, performing both pre-concentration and fluorination on the MDM platform

7. Analyzed the product by HPLC and determined its specific activity, radiochemical purity and radiochemical yield

8. Performed [^{18}F]fluoride pre-concentration and synthesis of rhodamine-^{18}F-ArBF_3 on the MDM platform and calculated the radiochemical purity of product.

Chapter 2. **Experimental**

In this chapter, we describe the materials used and the various experimental procedures including the Magnetic Droplet Microfluidics (MDM) method, synthesis of magnetic particles, pre-concentration of [^{18}F]fluoride by MDM, and radioactive synthesis of 3-formyl-2,4,6-trimethylbenzenesulfonyl [^{18}F]fluoride and rhodamine-^{18}F-ArBF_3.

2.1. Materials

All reagents were of analytical grade and they were used without further purification. Tetraethylorthosilicate (TEOS), iodomethane and K_2CO_3 were purchased from Caledon Labs. (3-aminopropyl)triethoxysilane (APTES) was purchased from MP Biomedicals. All other chemicals used (such as NaOH, acetonitrile, $FeCl_2$, etc.) were purchased from Sigma–Aldrich. The disc-shaped carrier magnet (5mm diameter x 1mm thickness) which was used to hold the magnetic particles was purchased from Indigo Instruments Inc. (Toronto) and Teflon sheet from Johnston Industrial Plastics, Ltd. (Toronto).

Deionized water (18 MΩ/cm) was used in all experiments unless otherwise stated. The precursor, 3-formyl-2,4,6-trimethylbenzenesulfonyl chloride (1) and the standard, 3-formyl-2,4,6-trimethylbenzenesulfonyl fluoride (3) was provided by Dr. Hua Yang from TRIUMF. The precursor, rhodamine aryltrifluoroborate (4), was provided by Dr. David Perrin from UBC.

2.2. Magnetic Droplet Microfluidics (MDM) Platform

The MDM platform consists of a robotic arm which was modified from an X-Y plotter (Figure 2.1). The movement of the arm and attached magnet was controlled by a

computer using Labview 8.2 software (National Instruments). A stage which held a Teflon sheet was placed above the robotic arm.

A camera was mounted above the MDM platform to record the droplet movement. A capillary tube, which was used to collect the $H_2{}^{18}O$ waste, was mounted on the surface and connected to a syringe pump. An image of the set-up is shown on Figure 2.2.

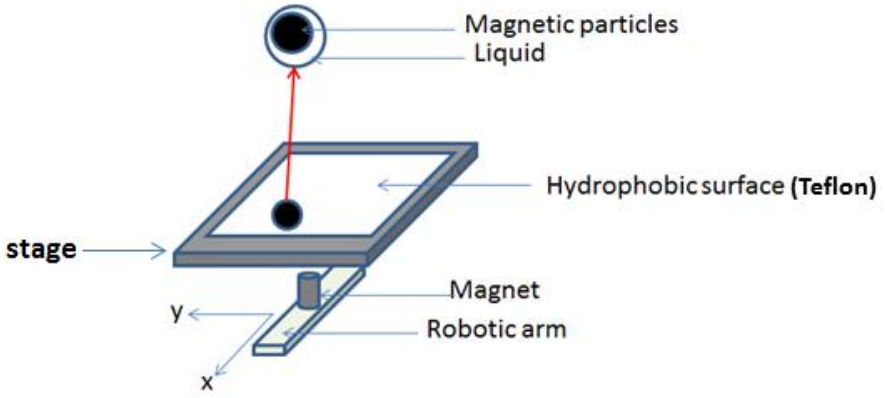

Figure 2.1 Schematic Diagram of Droplet Manipulation using magnetic particles on the MDM platform

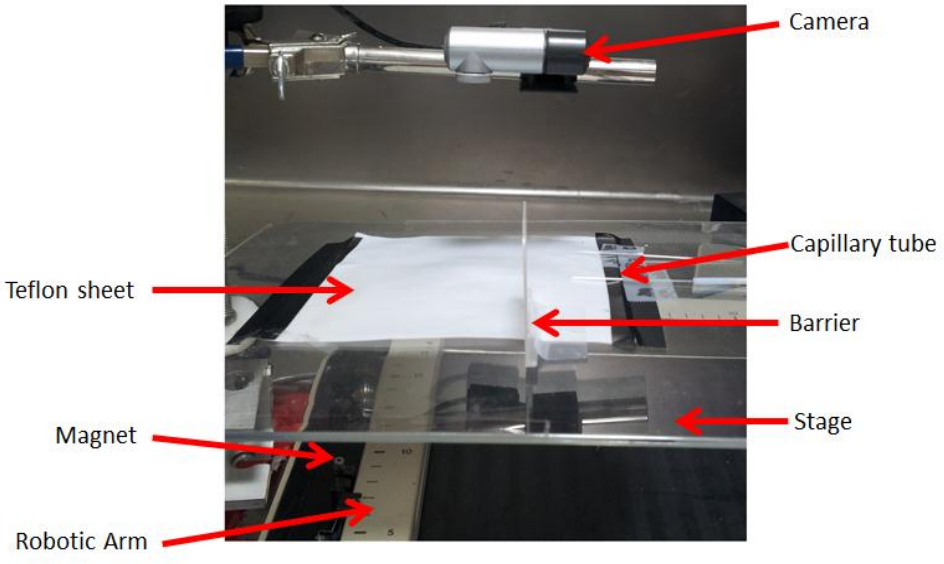

Figure 2.2 Photograph of the MDM platform
Note: The Teflon sheet was placed on the stage, and the robotic arm underneath the Teflon sheet to control movement of magnetic particles.

2.3. Synthesis of Quaternary methylammonium-modified Magnetic particles

2.3.1. Fe_3O_4 magnetic particles

Scheme 2.1 shows the chemical transformations for the production of the black magnetic (Fe_3O_4) particles. A $FeCl_2$ solution (0.24 M) of 22.5 mL was placed in a round-bottomed flask. The solution was mixed with polyvinyl alcohol (PVA) (1.50 g), which was previously dissolved in 30 mL water by heating at 95^oC. The resulting greenish-brown solution was sonicated at 50^oC for 10 min under nitrogen flow. An H_2O_2 solution (30 mL, 0.24 M) was then added dropwise to the mixture while stirred mechanically. NaOH (30 mL, 3M) was then added and the color of the solution immediately turned black. The solution was continuously stirred for 2 hours at ambient temperature under nitrogen flow. The solution was then transferred from the flask to a centrifuge tube and was centrifuged (using Centrifuge 5804, Eppendorf) at 10000 rpm for 20 min. The black particles were then collected with the aid of a magnet placed outside the tube.

$$2Fe^{2+}_{(aq)} + H_2O_{2(aq)} + 2H^{+}_{(aq)} \rightarrow 2Fe^{3+}_{(aq)} + 2H_2O_{(l)}$$

$$Fe^{2+}_{(aq)} + 2Fe^{3+}_{(aq)} + 8OH^{-}_{(aq)} \rightarrow Fe_3O_{4(s)} + 4H_2O_{(l)}$$

Scheme 2.1 Conversion of Fe^{2+} (from $FeCl_2$) to iron (II, III) oxide (Fe_3O_4)

The particles were washed with ethanol (30 mL) three times while the big particle chunks were broken apart into smaller ones using a glass rod. On the first batch, the breaking of the big chunks of particles was performed in open air and thus the process was done quickly to avoid oxidation of the particles since they were exposed to air. Because of the short time available, the particles were not broken evenly and the particle sizes were large. To allow for a longer time for breaking the large particles, this process was conducted inside a glove bag filled with argon to prevent oxidation. In this way, smaller-sized particles were obtained and they remained black and magnetic for a long time.

2.3.2. Silica coating of Fe_3O_4 particles

The magnetic particles were then coated with silica to protect against oxidation (Bruce et al., 2004). The resulting black magnetic particles were stirred with 150mL of ethanol, mixed with 12 mL of ammonium hydroxide (28%-30% NH_3) under N_2 flow. Then, 400µL of tetraethylorthosilicate (TEOS) was added dropwise to the liquid mixture to produce silica (SiO_2) on the particle surface. The chemical equation of silica formation is shown in Scheme 2.2. Ammonium hydroxide was added to make the solution basic in order to allow for the displacement of the tetraethoxy ($-OC_2H_5$) moiety. The particles were then separated from the liquid using a magnet and they were washed with ethanol (30 mL) three times. The above steps were repeated twice to ensure that the particle surfaces were sufficiently coated with silica. The silica-coated particles were washed with ethanol and then collected from the solution with the aid of a magnet. The particles were stored dry until the next step.

$$Fe_3O_{4(s)} + Si(OC_2H_5)_{4(aq)} + 2H_2O_{(l)} \rightarrow Fe_3O_4\text{–}SiO_{2(s)} + 4C_2H_5OH_{(aq)}$$

Scheme 2.2 Silica formation for coating on the Fe_3O_4 particle surface

2.3.3. Synthesis of 3-aminopropyl-modified Fe_3O_4

To introduce a primary amine group on the surface of the silca-coated particles, (3-aminopropyl)triethoxysilane (APTES) solution was used to react with the silanol groups on the silica surface of the particles. The activation of silanol groups on the silica surface is shown in Scheme 2.3A. Briefly, silica-coated Fe_3O_4 was stirred with HCl (20 mL, 5% v/v) for 20 minutes to activate surface silanol groups. Then, the particles were washed with ethanol (30 mL) until the solution pH dropped to 4-5. 20 mL of anhydrous ethanol was added to the magnetic particles followed by the addition of 4 mL of APTES. The reaction between silanol and APTES is shown in Scheme 2.3B. The solution was refluxed for 3 hours at 60^{o}C (The procedure is adapted from a previous report, Liu et al., 2011). After heating, the particles remained black and these were washed with 50 mL chloroform to remove unreacted APTES.

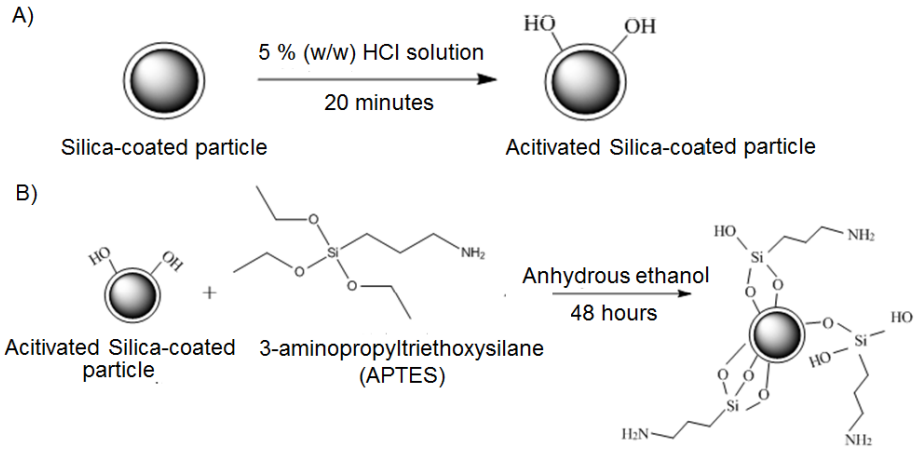

Scheme 2.3 APTES attachment on the surface of the magnetic particles: A) Silica-coated Fe_3O_4-based particles were activated with HCl solution to produce surface silanol groups. B) The amine group was attached on the surface by reacting the activated particles with 3-aminopropyltriethoxysilane (APTES)

2.3.4. Conversion of 3-aminopropyl-coated Fe_3O_4 particles to trimethyl ammonium iodide

To introduce the ion-exchange function on the magnetic particles, the primary amine on the particles was converted to a quaternary methylammonium iodide (Scheme 2.4). First, the amine-functionalized particles were added to 50 mL acetonitrile in a flask that contained 5.0 g K_2CO_3 and 1.50 mL CH_3I. The mixture was refluxed at 70-75^oC for 20 hours. The flask was covered with aluminum foil to prevent photo-oxidation of iodide to iodate. The black particles were then separated from the solution with the aid of a magnet and they were washed with dichloromethane.

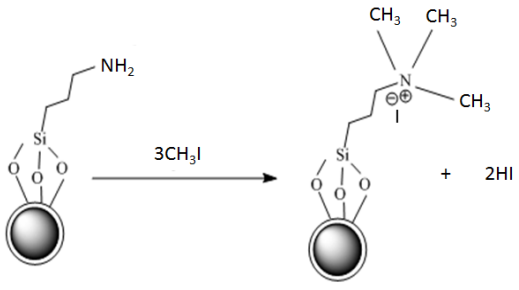

Scheme 2.4 Conversion of primary amine to quaternary methylammonium iodide

2.4. Pre-concentration of [^{18}F]fluoride on the MDM platform

High-energy protons (13 MeV) were produced on a TR13 cyclotron at TRIUMF. [^{18}F]F^- was produced by proton bombardment (10 microamps, 5 minutes) on 1 mL of [^{18}O]H_2O, see Scheme 2.5. No [^{19}F]F^- has been added and so this process is called no-carrier-added.

$$^{18}_{8}O + ^{1}_{1}p \rightarrow ^{18}_{9}F + ^{1}_{0}n$$

Scheme 2.5 Proton Irradiation of $H_2{}^{18}O$ target to produce no-carrier-added [^{18}F]F^-

Typical production of [^{18}F]F^- saw 40.5-70.2 mCi (1.5–2.6 GBq) at the end of bombardment (Inkster et al., 2012). The activity of the [^{18}F]fluoride solution produced was measured with a gamma detector (Capintec, CRC-127R Dose Calibrator) which had an automatic zeroing function and background correction. For safety reasons, an aliquot with an activity of approximately 2 mCi was taken. This aliquot was diluted to a volume of 1 mL for the fluoride pre-concentration experiment.

The MDM platform was set up as previously described in Figure 2.1 and 2.2. The step-by-step operation procedures are depicted in Figure 2.3. In step 1, the magnetic particles (***A***), approximately 25 mg, were adhered into a disc-shaped carrier magnet (5 mm diameter, 1mm thickness) and placed on the platform. This carrier magnet held the magnetic particles and allowed them to be moved as a group. One mL of $^{18}F/H_2{}^{18}O$ solution was placed as 2 separate droplets (500 µL each) on the platform. This step was used to increase the surface area of the liquid and also because smaller droplets are less likely to scatter on the platform. In step 2, the magnetic particles were dragged towards the first $^{18}F/H_2{}^{18}O$ droplet, controlled through the Labview 8.2 software. The magnetic particles were looped around the droplet to induce a stirring effect. This continuous looping was also computer-controlled and this operation could be stopped at a desired time. Once the desired operation time (e.g. 2 min.) was reached, the particles were moved towards the capillary tube for removal of the $H_2{}^{18}O$ (***B***) waste (in steps 2-4). Steps 2 -4 were performed repeatedly until $H_2{}^{18}O$ (***B***) was completely removed. [^{18}F]fluoride ions captured by the quaternary ammonium groups on the particles were

released using 50µL of K_2CO_3 (***C***) solution (steps 5-6). This release step was conducted at two different K_2CO_3 concentrations (0.0774 M and 0.145 M).

The activity of the $H_2{}^{18}O$ solution collected in the capillary tube was also measured. The activity of [^{18}F]fluoride left on the particles and the activity of [^{18}F]fluoride released into the solution were both measured. Radioactive experiments were all conducted in a lead-shielded hot cell in TRIUMF.

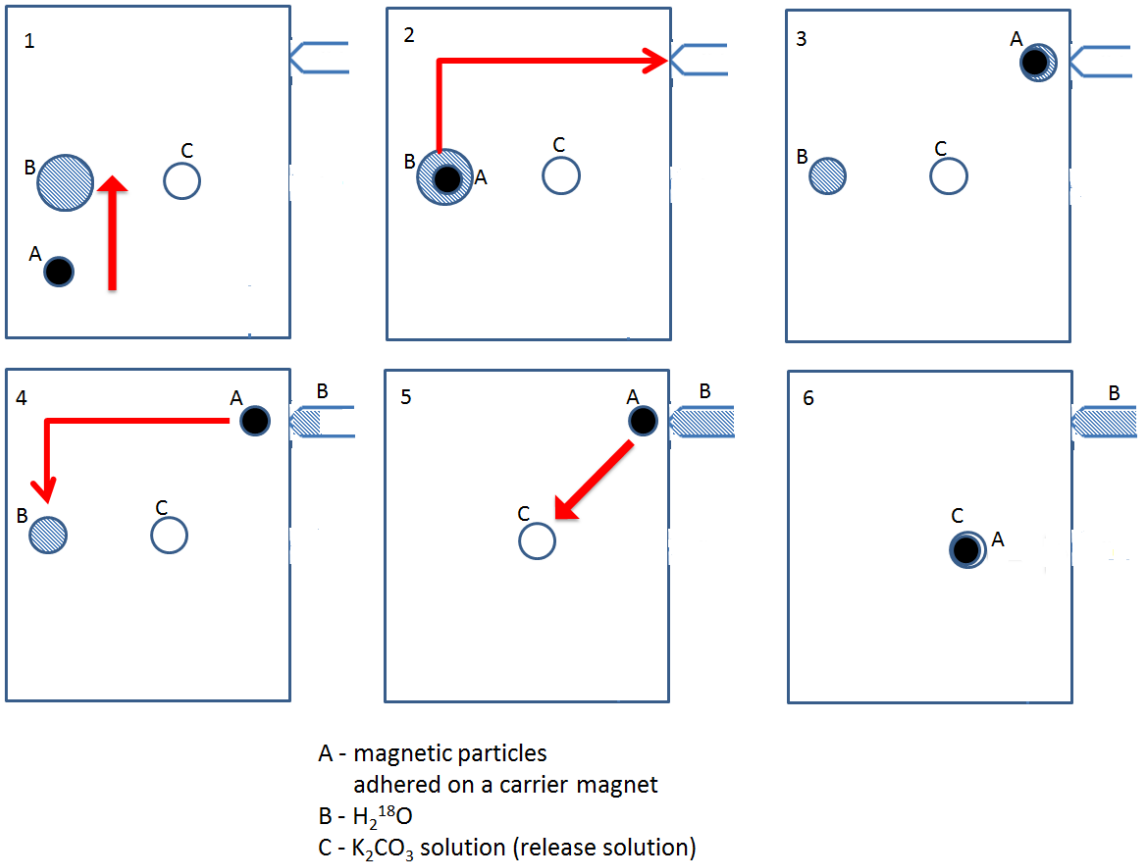

Figure 2.3 Steps for [^{18}F]fluoride pre-concentration on the MDM platform
Note: 1) The magnetic particles (***A***) were moved towards the $H_2{}^{18}O$ solution (***B***) that contains [^{18}F]F^- ions. The particles were looped in a circular motion within the solution to induce stirring motion. 2) The particles were moved towards the capillary tube carrying a droplet of $H_2{}^{18}O$. 3) [^{18}F]F^- will stay on the magnetic particles and the $H_2{}^{18}O$ droplet was collected by the capillary tube. 4) The particles were moved back to the $H_2{}^{18}O$ solution to carry another droplet. Steps 2-4 was repeated continuously until $H_2{}^{18}O$ was completely consumed 5) The particles moved toward K_2CO_3 solution (***C***) to release [^{18}F]F^- ions. The particles containing the [^{18}F]F^- ions again looped in a circular motion within the solution to induce stirring motion. 6) The pre-concentrated [^{18}F]F droplet was then pipetted out from the platform and the activity of the sample was measured.

2.5. Synthesis and analysis of 3-formyl-2,4,6-trimethylbenzenesulfonyl [^{18}F]fluoride (2) on the MDM platform

The radioactive 3-formyl-2,4,6-trimethylbenzenesulfonyl [^{18}F]fluoride (2) was prepared by reacting precursor, 3-formyl-2,4,6-trimethylbenzenesulfonyl chloride (1) (dissolved in tBuOH) with [^{18}F]fluoride (Scheme 1.13 in Section 1.3.2).

The preparation of the precursor, and the synthesis of the reference standard, 3-formyl-2,4,6-trimethylbenzenesulfonyl [^{19}F]fluoride was synthesized as described in Inkster et al., 2012.

2.5.1. Use of 3-formyl-2,4,6-trimethylbenzenesulfonyl [^{19}F]fluoride as a standard for HPLC analysis

To prepare the stock solution of [^{19}F]-(2), 4.60 mg of the compound was dissolved in 10 mL of acetonitrile (2 mM). This stock solution was serially diluted into 3 concentrations using acetonitirile, and an aliquot (25 µL) of each was assayed by analytical HPLC. HPLC conditions are as follows: column: C-18, UV Detector: 254 nm; isocratic elution, 70:30 MeCN: 0.1 % trifluoroacetic acid (TFA), flow rate = 1 mL/min.

25 µL of each aliquot was injected three times and the UV absorbance at 254 nm of peak at 10.9 min. retention time was measured. The average absorbances were plotted against each concentration and a linear plot of peak area vs. concentration was generated, see Appendix, Section A.5.1 for details.

2.5.2. Synthesis of [^{18}F]-(2) on the MDM platform

The pre-concentration step and the synthesis reaction were both conducted on the MDM platform. The same steps outlined in Figure 2.3 were performed here except that droplet (***C***) now contained both the releasing solution and the precursor (1). First, 50 µL of pre-concentrated [^{18}F]fluoride [as prepared in Section 2.4 using ~2 mCi of [^{18}F]fluoride and aqueous K_2CO_3 (0.0145 M)] was allowed to react with 50 µL of 3-formyl-2,4,6-trimethylbenzenesulfonyl chloride (1) (3 µmol, 0.060 M), in *t*-BuOH. Final reaction

volume was 100 µL and the final concentration of (1) was 0.030 mM. The reaction was allowed to proceed for ~5 min. Here, the capture/release of [^{18}F]fluoride ions and the synthesis reaction was done on the same platform to synthesize the product, [^{18}F]-(2).

The product mixture was then collected from the MDM platform and then manually transferred into a SPE column (tC18 'light') to remove excess fluoride and tBuOH. Before use, the column was activated with EtOH (2 mL) and water (6 mL), then washed with water (5 mL), and dried with air.

After purification of [^{18}F]-(2), an aliquot (40 µL) of known activity was assayed by HPLC using both the UV absorbance detector and the radioactive detector. The amount of [$^{18/19}$F]-(2) and the total activity of the sample were used to calculate the specific activity of [^{18}F]-(2) (see Appendix, Section A.5.2).

2.6. Synthesis of rhodamine-[^{18}F]-ArBF$_3$ (5)

The synthesis of rhodamine-[^{18}F]-ArBF$_3$ (5) (see Scheme1.11) was performed by the conventional method and by the MDM platform. The conventional radiosynthetic method was first performed by following similar procedures described in Liu et al. (2012).

2.6.1. Conventional Synthesis of rhodamine-[^{18}F]-ArBF$_3$

For the conventional synthesis of [^{18}F]-(5), low quantities (~5 mCi) of [^{18}F]fluoride were used in the reaction and no drying step was performed. A quaternary methylammonium (QMA) anion exchange column (ORTG, Inc.) was used to pre-concentrate the [^{18}F]fluoride solution.

The QMA column was pre-treated with (i) deionized (DI) water (6 mL); (ii) saturated brine (26% w/w, 6mL); and (iii) DI water (6mL). About 30 mCi of no-carrier-added [^{18}F]F$^-$ solution produced from the cyclotron was passed through the QMA column. [^{18}F]F$^-$ was then eluted using 0.20 mL, $NaClO_4$ (0.0817 M) in water and collected into a plastic polypropylene vial. Since a low activity was desired to perform the synthesis, approximately 0.05 mL of the pre-concentrated [^{18}F]fluoride solution (~5 mCi)

was withdrawn from this vial and the solution was added to another vial containing 20 µL [^{19}F]-(4) (50 nmol in acetonitrile),10 µL of pyridazine-HCl (2M, pH2) buffer and 1 µL KHF_2 (17.5 nmol). The reaction mixture was agitated using a vortex mixer for ~1 min and then the vial was placed in a heating block set at 40^{o}C. After 10–15 min, the vial was removed from the heating block and the reaction was quenched by the addition of 1mL of NH_4OH (5% in 50:50 MeCN/H_2O). The addition was achieved via a syringe to resuspend the contents of the product mixture. From this mixture, a small volume of 50 µL was taken for HPLC analysis.

2.6.2. Synthesis of rhodamine-[^{18}F]-$ArBF_3$ (5) on the MDM platform

In addition to the MDM set up that is shown in Figure 2.2, a heating lamp was installed above the stage since the synthesis reaction requires higher temperature as reported by Liu et al. Prior to the experiment, the temperature in the platform was calibrated to 40^{o}C using a thermocouple thermometer. A plastic petridish was placed as a cover on the Teflon surface on the stage to prevent possible evaporation of the liquid droplet when temperature is 40^{o}C (Figure 2.4).

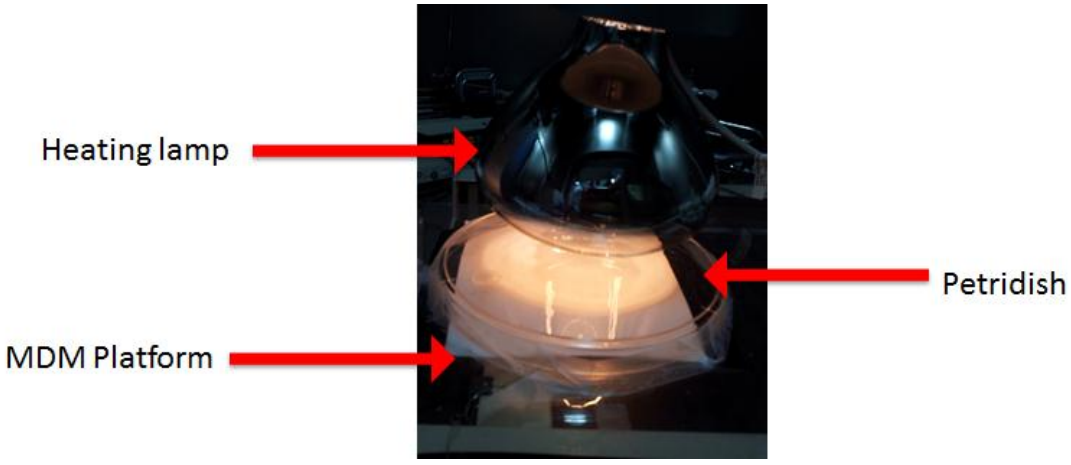

Figure 2.4 Heating lamp was installed on the platform to heat the reaction to 40^{o}C. A petridish was also placed on the platform to cover the droplets and minimize liquid evaporation

For the synthesis reaction, 50 nmol of precursor, [^{19}F]-(4) in 20 µL acetonitrile was mixed with 1 µL of 17.5 nmol of KHF_2 and 10 µL of pH 2 buffer (2M pyridazine-HCl). This precursor solution was loaded into a 1-mL syringe just prior to the start of

experiment. [^{18}F]fluoride pre-concentration was performed as described in section 2.4 using quaternary ammonium tagged magnetic particles. [^{18}F]F^- ion captured on the particles was released using 50 µL of the $NaClO_4$ (0.0817 M) solution. The pre-concentrated [^{18}F]fluoride (50 µL) was then collected on the same syringe where the precursor solution was loaded. The used particles were then discarded. Silica-coated magnetic particles were not allowed to react with the pH 2 solution to avoid reaction of HF and the silica coating. Thus, after the [^{18}F]fluoride and the precursor solution in the syringe was pumped out (flow rate: 1 mL/min) into the platform, only the magnetic carrier bead (no magnetic particles) was used to induce stirring on this droplet. The temperature on the platform was maintained at 40 ± 1 ^{o}C during the 10-15 min reaction time. After the reaction was quenched by the addition of 1 mL of NH_4OH (5% in 50:50 MeCN/H_2O), a small volume of 50 µL was removed from the product mixture (using a syringe) for activity measurement and it was injected for HPLC analysis. Figure 2.5 illustrates the step-by-step process of the synthesis of [^{18}F]-(5).

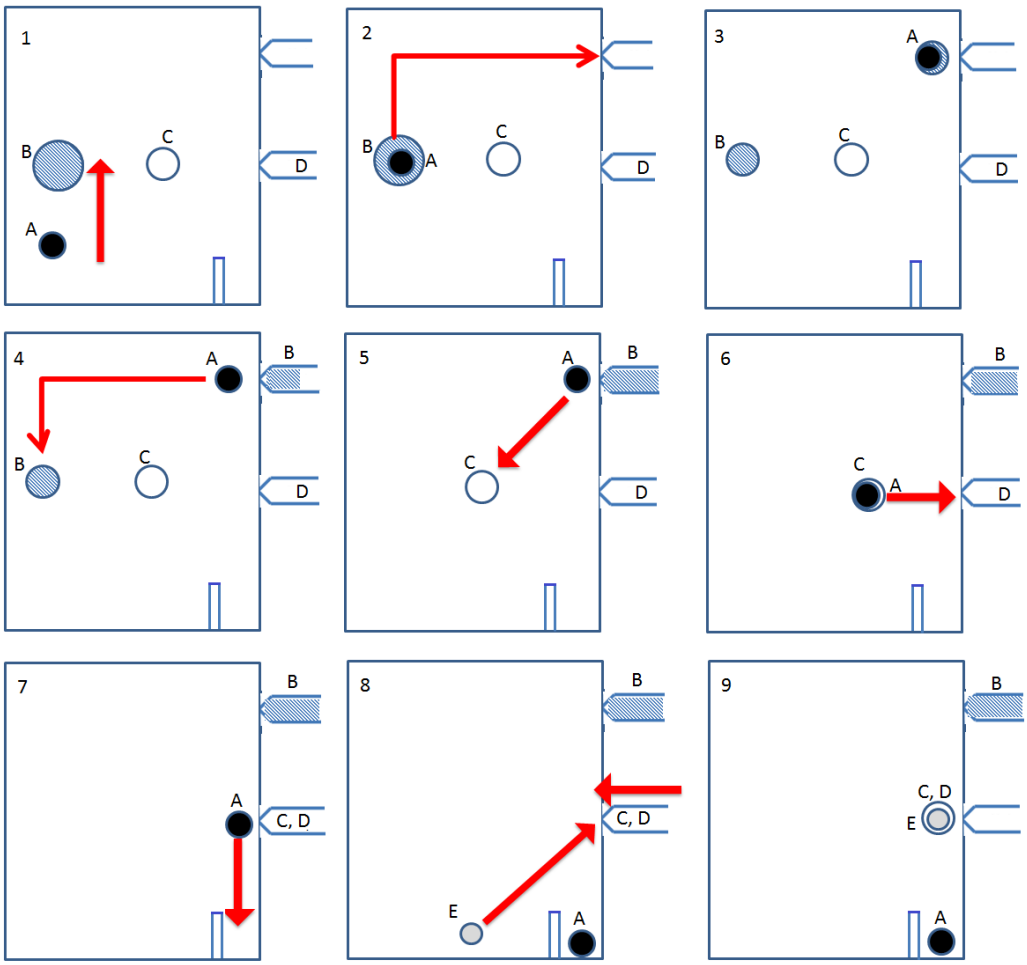

Figure 2.5 Steps for pre-concentration of [^{18}F]fluoride and subsequent synthesis of [^{18}F]-(5)

Note: 1) The magnetic particles (***A***) were moved towards the $H_2{}^{18}O$ (***B***) solution that contains [^{18}F]F$^-$. The particles were then looped in a circular motion within the solution to induce stirring motion. 2) The particles were moved towards the capillary tube carrying a droplet of $H_2{}^{18}O$ solution. 3) This droplet was collected by the capillary tube. 4) The particles were moved back to the $H_2{}^{18}O$ solution to carry another droplet. Steps 2-4 was repeated continuously until $H_2{}^{18}O$ solution was completely removed 5) The particles were moved toward $NaClO_4$ solution (***C***) to release [^{18}F]F$^-$ ions. The particles were again continuously looped in a circular motion within the solution to induce stirring motion 6) The particles then carried the pre-concentrated [^{18}F]F solution (50 µL) to be collected on the syringe containing the precursor mixture (***D***) (containing [^{19}F]-(4), KHF_2, pH2 buffer). 7) Particles were moved to the barrier. 8) The precursor mixture (***D***) inside the syringe was then pumped out into the platform by a syringe pump. The robotic arm picked up the carrier bead then moved towards (***C***) and (***D***) to loop around the droplet and induce stirring motion. This was done 10-15 min at 40^{o}C. The product was then be collected by a 1-mL syringe.

Chapter 3. **Results and Discussion**

3.1. Synthesis of Quaternary methylammonium-modified Magnetic Particles

The surfaces of magnetic particles were modified to contain F^- anionic exchange functional groups in order to capture ^{18}F ions in a liquid droplet. Since these particles were magnetic, they can be manipulated by the use of a magnet to facilitate the movement of the particles on the MDM platform.

The preparation of Fe_3O_4 particles was conducted under an inert gas atmosphere. Polyvinylalcohol (PVA) acts as a protective agent to stabilize the colloidal dispersion of Fe_3O_4 and prevent its oxidation to Fe_2O_3 (Lee et al., 1996). In addition, the silica coating is used to provide protection for Fe_3O_4 from being oxidized to Fe_2O_3 (scheme 3.1), which is brown in color and has no magnetic properties.

$$2Fe_3O_{4(s)} + ½\ O_{2(g)} \rightarrow 3Fe_2O_{3(s)}$$

Scheme 3.1 Reaction of Fe_3O_4 with O_2 to form Fe_2O_3

After the particles were coated with silica, it was occasionally found that the particles still underwent oxidation to Fe_2O_3, see Figure 3.1A. This problem may be caused by the porous nature of the silica coating (Bruce et al., 2004). Based on our previous experience, either black or brown particles were obtained when only one silica deposition cycle was performed. Therefore, we decided to perform two cycles of depositions, and we then consistently obtained black Fe_3O_4 magnetic particles (Figure 3.1B) without oxidation. We found that these doubly coated particles remained black even after 3 months or longer. These particles were stored in a tightly covered glass container which was sealed with a paraffin film.

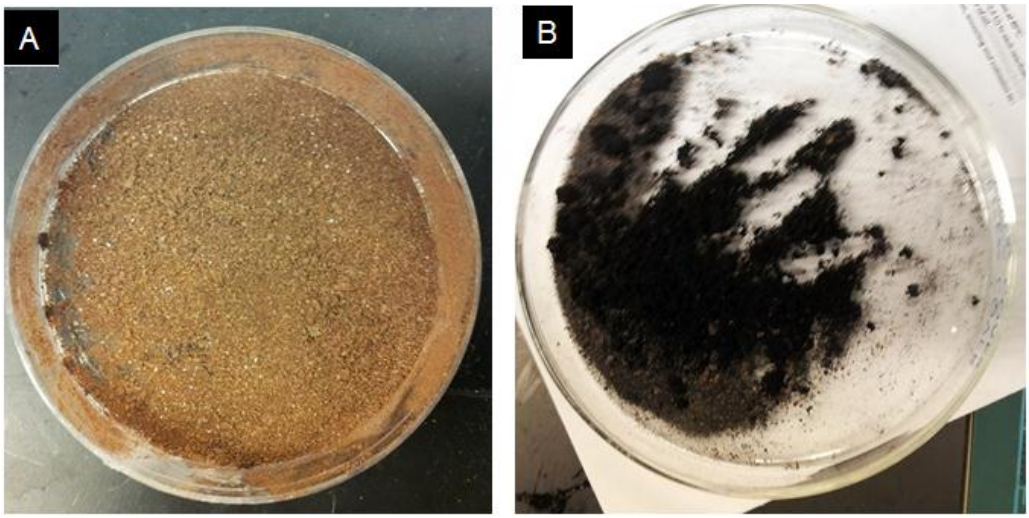

Figure 3.1 (A) Only one silica coating resulted in particles turning brown (Fe_2O_3) (B) Double-coated silica particles consistently produced stable black (Fe_3O_4) particles

After silica coating, the next step was to activate the silanol groups on the silica surface with HCl. These silanol groups were needed to append the amine groups on the particle surface using APTES. The primary amine that was attached on the silica surface is then methylated by reacting the amine with 3 equivalents of methyl iodide (CH_3I), see Scheme 2.4. The reaction of a primary amine (RNH_2) with CH_3I involves the formation of a secondary amine (RR'NH) and the liberation of HI which combines with the secondary amine to form the amine hydroiodide salt ($RR'NH_2^+I^-$). Consequently, very low concentrations of free amines remain for subsequent alkylation to give the tertiary and quaternary amine. To increase the concentration of the free amines, an inorganic base is utilized as the proton acceptor to capture HI. Thus, a common protocol includes the presence of an inorganic base like K_2CO_3 in a polar aprotic solvent such as MeCN (Sommer et al.,1969). In this way, the equilibria (as shown in Scheme 3.2) can be shifted toward complete alkylation of the primary amine to produce the quaternary ammonium ($[RR'_3N]^+I^-$) salt.

The structure of the quaternary amine modified magnetic particles is shown in Scheme 3.3. The quaternary amine served as the ion-exchanging group and it can be utilized to capture [^{18}F]fluoride ion, liberating the iodide ion.

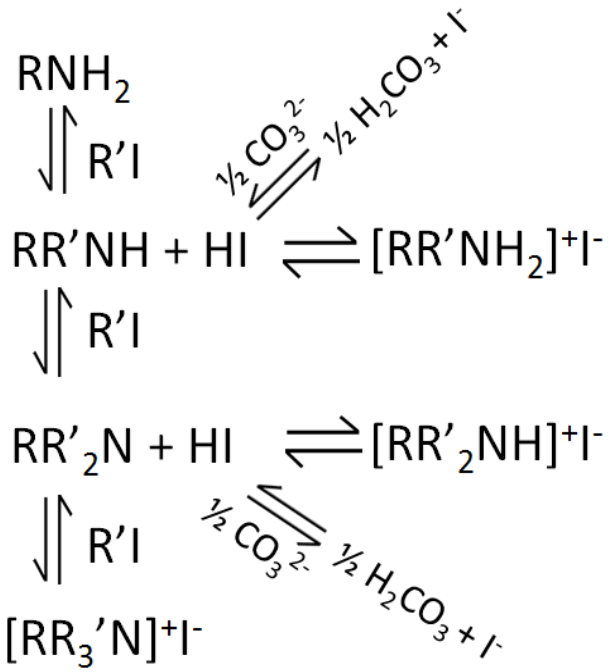

Scheme 3.2 **Reaction of a primary amine with an alkylating agent (such as CH_3I). A sequence of reactions occurs resulting in the formation of a mixture of products. The equilibria can be shifted toward complete alkylation by the introduction of an inorganic base such as K_2CO_3 to remove HI (Sommer et al.,1969)**

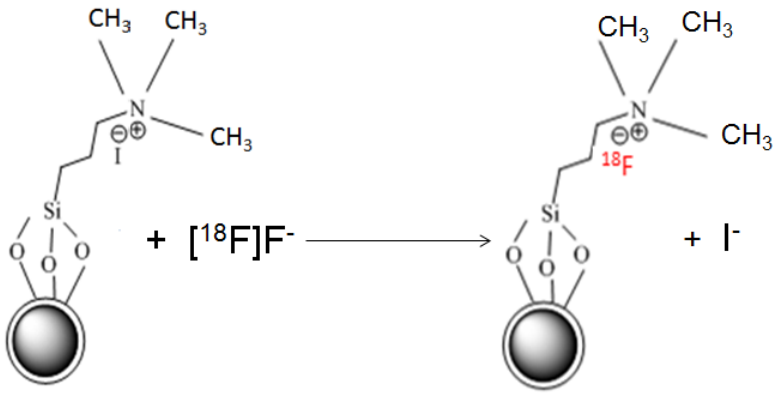

Scheme 3.3 **F^- ion-exchanging Fe_3O_4 particles which can capture [^{18}F]fluoride**

An elemental analysis was performed on the particles by the energy-dispersive X-ray (EDX) scan (conducted on a scanning electron microscope (SEM)) to characterize the elements present in the sample. Figure 3.2A shows that iodine (I), which was

expected to be present on the surface of the quaternary ammonium iodide tagged particle, was initially present on the first EDX scan on the particles. These particles were then allowed to react with NaF solution (0.01 mM, 10 mL) to capture F^-. Fluoride was released using a $NaClO_4$ solution (0.0817 M, 0.2 mL). After performing the ion-exchange reaction, a second scan (Figure 3.2B) was conducted on the particles. It clearly showed that the iodine signal was no longer present, having been replaced by the signal for chlorine, which is believed to come from ClO_4^-.

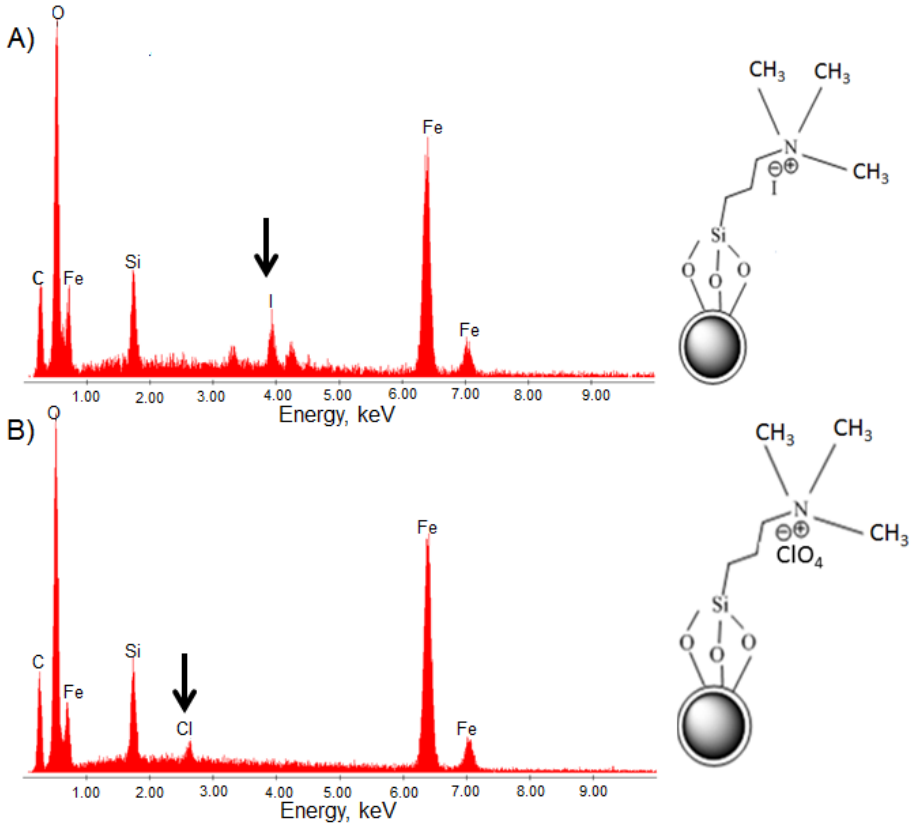

Figure 3.2 Energy-dispersive X-ray (EDX) Spectrum for quaternary methylammonium iodide-functionalized particle

Note: A) Before fluoride capture, the signal for iodine (indicated by an arrow) was present on the spectrum and B) after fluoride capture and subsequent exchange by ClO_4^- to release fluoride, the signal for iodine was not present but replaced with chlorine (indicated by an arrow).

The particles were also observed and their sizes measured using a Nikon Eclipse TE300 microscope. As discussed in Section 2.3.1, the particles obtained in the initial trials were bigger and their sizes ranged between 200-250 µm (Figure 3.3A). When the

particles aggregates were ground, 50-100 µm particles (Figure 3.3B) were isolated. The process of breaking the big particles to smaller ones is time-consuming and therefore it is important to make sure that the particles are not exposed to oxygen during the procedure. This process was performed inside a glove bag under argon and it took less than an hour to complete.

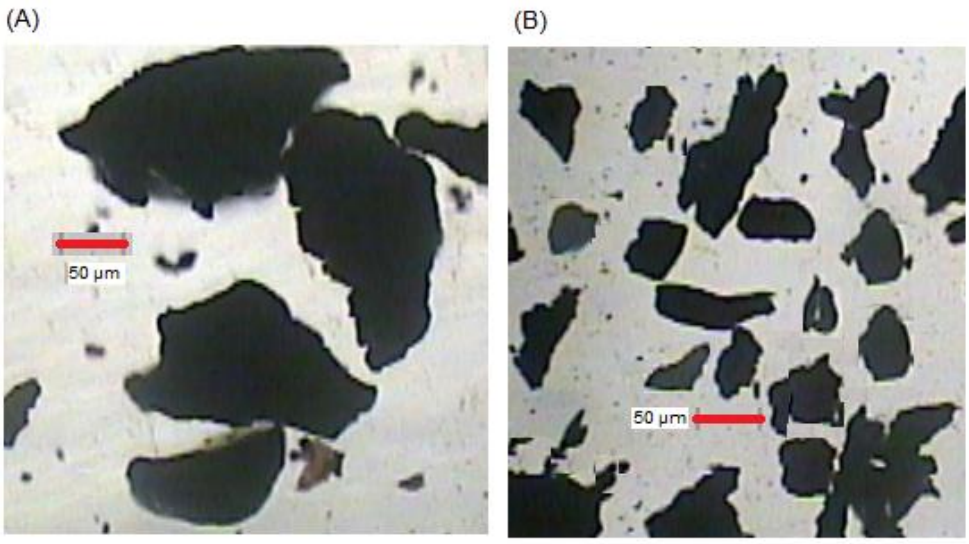

Figure 3.3 Image of magnetic particles using 5x microscopic objective lens: (A) Big-sized particles (B) Small-sized particles were achieved by grinding the big-sized particles under Ar in a glove bag. Scale bar is 50 µm.

The masses of the magnetic particles obtained after each step are tabulated in Table 3.1. The total mass of magnetic particles collected was 400-450 mg per batch for the big particles while 320-360 mg per batch for the smaller particles. Lower yields were isolated in the preparation of small-sized particles (50-100 µm) due to significant losses during processing.

Table 3.1 Masses of magnetic particles in every step per batch

Size of Particles	200-250 µm	50-150 µm
Fe_3O_4 (Section 2.3.1)	490 ± 20 mg	450 ± 20 mg
Silica-coated Fe_3O_4 (Section 2.3.2)	470 ± 20 mg	410 ± 20 mg
Formation of amine group (Section 2.3.3)	465 ± 15 mg	385 ± 15 mg
Formation of Quaternary Ammonium ion (Section 2.2.4)	430 ± 20 mg	340 ± 20 mg

Errors are SD (n>5).

3.2. Capture and Release Efficiency of Quaternary methylammonium-modified particles vs. Operation time on MDM

The pre-concentration of [^{18}F]fluoride was performed using the steps illustrated in Figure 2.3 in the MDM. Each run of [^{18}F]fluoride capturing was conducted using 25 mg NR_4^+-modified magnetic particles in 1 mL volume of [^{18}F]fluoride/$H_2{}^{18}O$ with initial radioactivity of 2-5 mCi. After $H_2{}^{18}O$ was removed, 50 µL of K_2CO_3 (0.0145 M) was used to release [^{18}F]F^-. Activity measurements were taken in four areas to assess the capture and release efficiency. First was the initial [^{18}F]fluoride/$H_2{}^{18}O$ solution, second was the $H_2{}^{18}O$ waste collected in the capillary tube, third was the activity left on the magnetic particles after F^- release and fourth was the pre-concentrated ^{18}F released with K_2CO_3. All measurements were decay-corrected to EOB, see Appendix, Section A.1. The capture efficiency is calculated from the initial [^{18}F]fluoride/$H_2{}^{18}O$ activity and the activity of the collected $H_2{}^{18}O$ (Equation 3.1). The release efficiency is calculated from the activity of released [^{18}F]fluoride and the activity left on the magnetic particles (Equation 3.2). A sample calculation of the capture efficiency and release efficiency is shown in Appendix, Section A.2.

During the capture and release steps, the magnetic particles were allowed to loop in a circular motion within the liquid droplet to induce stirring. This procedure was conducted at different operation times (2 to 8 min.). The capture and release efficiencies are plotted against different operation times, as shown in Figure 3.4. There was an increase of both capture% and release % when the operation time was increased to 2 min. The efficiencies are 79 ± 3 % and 93 ± 3 %, respectively (n=3), see Figure 3.4. When the operation time was increased further to 4 min. and 8 min., no improvement was observed. Thus, the optimum operation time was taken to be 2 min. for both the capture and release steps.

Equation 3.1. Calculation of Capture Efficiency

$$\text{Capture Efficiency} = \frac{\text{Initial } {}^{18}\text{F}/H_2{}^{18}O \text{ activity} - \text{Activity in } H_2{}^{18}O \text{ waste}}{\text{Initial } {}^{18}\text{F}/H_2{}^{18}O \text{ activity}} \times 100\%$$

Equation 3.2 Calculation of Release Efficiency

$$\text{Release Efficiency} = \frac{\text{Activity in released solution}}{\text{Initial } {}^{18}F/H_2{}^{18}O \text{ activity} - \text{Activity in } H_2{}^{18}O \text{ waste}} \times 100\%$$

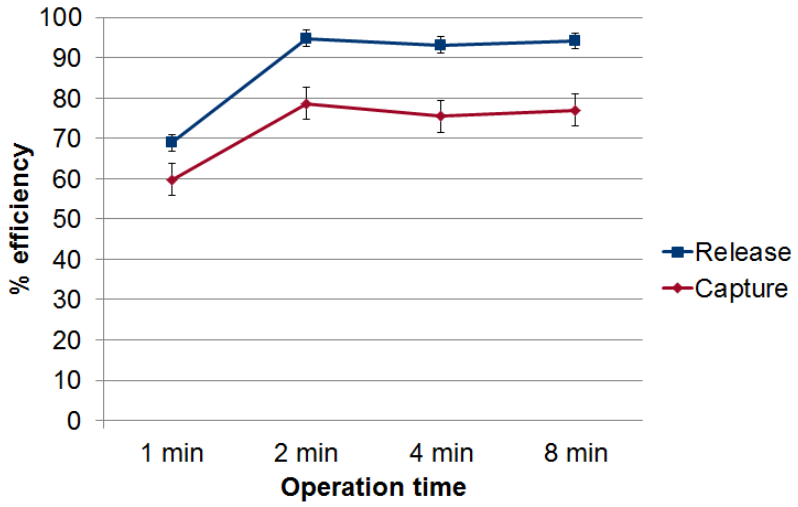

Figure 3.4 Capture efficiency and Release efficiency plotted against operation time

Note: Operation time is the time the particles were allowed to loop on a circular motion within the droplet to induce stirring. Initial activity of $^{18}F/H_2{}^{18}O$ was ~2 mCi and particle size was 50-100 µm. Releasing agent used: 50 µL K_2CO_3 (0.145 M). Error bars represent SD (n =3).

3.3. [^{18}F]fluoride Capture Efficiency of Quaternary methylammonium-modified particles vs. the amount of fluoride ions in solution

Based on the results in Section 3.2, the highest capture efficiency achieved was 79 ± 3% (see Figure 3.4). This observation may be attributed to the saturation of the ion-exchange sites on the particles. Therefore, the [^{18}F]F^- ion-exchange capacity of 25 mg of particles was investigated by varying the initial activity of [^{18}F]fluoride/$H_2{}^{18}O$ thereby varying the initial amount of [^{18}F]F^- ions in the solution.

We believe that the large particle size may also result in the saturation of the F^- ion-exchanging capacity of the particles, and so particles of two different sizes were analyzed. The first batch of particles has a bigger size (200-250 µm). An operation time

of 2 minutes on the MDM was used in this experiment. From Table 3.2, it was found that when the initial ^{18}F activity was increased (thereby increasing mass of fluoride), the capture efficiency decreased. This trend can be explained by the fact that, the ion-exchange sites on the particles are more likely to be occupied and became saturated as the amount of fluoride increases.

Since we believe that the ion-exchanging capacity of the particles may increase as the particle size is reduced, leading to a greater surface area for the formation of $NR_4^+I^-$, we decide to make smaller particles. It must be noted in Section 2.3.1 that breaking of the particles to smaller sizes was performed before silica coating and functionalization of the particle surface. Thus, it is expected that as the size of the particle was decreased, the particle surface area increased, and this should lead to a greater availability of ion-exchange sites on the surface. The mass of fluoride was estimated assuming that the specific activity of [^{18}F]fluoride produced from the TR-13 cyclotron is approximately 2 Ci/μmol (Futchner et al., 2008), see Appendix, Section A.3. From Table 3.2, the particles with a smaller size were observed to produce a higher capture efficiency. This efficiency further increased when the amount of fluoride is less.

Table 3.2 Effect of the activity of [^{18}F]fluoride solution and particle size on the capture efficiency of 25 mg quaternary methylammonium tagged magnetic particles

Size of Particles	Initial activity, mCi	Mass of F^- ions, μg	Capture Efficiency
200-250 μm	1.86 ± 0.02	0.018 ± 0.001	86 ± 3
	2.56 ± 0.02	0.024 ± 0.001	70 ± 3
	6.91 ± 0.02	0.066 ± 0.001	63 ± 2
50-100 μm	1.96 ± 0.02	0.019 ± 0.001	93 ± 3
	3.50 ± 0.02	0.033 ± 0.001	79 ± 3
	6.97 ± 0.02	0.066 ± 0.001	59 ± 3

The error is SD (n=3). Sample calculation of capture efficiency is shown in Appendix, Section A.2 and all activities were decay corrected to EOB. Calculation of the mass of fluoride ions is based on the activity of ^{18}F and decay constant, see Appendix, Section A.3 for sample calculation.

When an initial activity of 30-33 mCi of [^{18}F]fluoride/$H_2{}^{18}O$ was used, the capture efficiency using 25 mg of magnetic particles (50-100 μm) was 35 ± 3% (Table 3.3). This value is smaller than 59 ± 3 % when 6.97 mCi of initial activity was used (see Table 3.2). This observation was expected because the ion-exchange sites on the particles were

already saturated even when 6.97 mCi was used and so the use of 30-33 mCi could not lead to any further capture. On the other hand, when the mass of the magnetic particles was increased to 40 mg, the capture efficiency increased from 35 ± 3% to 51 ± 3%. These results support the observation in Table 3.2 that the capture efficiency is dependent on the number of ion-exchange sites on the surface of the particle.

Table 3.3 Effect of scaling up the [^{18}F]fluoride activity to 30-33 mCi and doubling the mass of particles on the capture efficiency of quaternary ammonium tagged magnetic particles

Size of Particles, µm	Mass of Particles Used, mg	Activity, mCi	Mass of ^{18}F ions, µg	Capture Efficiency, %
50-100	25 ±1	32 ± 2	0.300 ± 0.02	35 ± 3
	40 ± 1	32 ± 2	0.300 ± 0.02	51 ± 3

The errors are SD (n=3).Sample calculation of mass is shown in Appendix, Section A.3. All activities used are decay-corrected to EOB.

3.4. [^{18}F] Release Efficiency obtained with K_2CO_3

After the magnetic particles capture the fluoride ion, we are able to release [^{18}F]F^- ions in a solution through a second ion exchange reaction as shown below:

$$R_4N^+ F^- + X^- \underset{}{\overset{H_2O}{\rightleftharpoons}} R_4N^+ X^- + F^-$$

Scheme 3.4 Ion exchange reaction of quaternary methylammonium fluoride to release F^- ions

The carbonate anion in K_2CO_3 is used to release [^{18}F]F^-. K_2CO_3/Kryptofix 2.2.2 (K2.2.2) in acetonitrile:water has long been used as an eluent to elute fluoride ions on an [^{18}F]fluoride trap and release column. In the mixture, the cryptand K2.2.2 is used to increase nucleophilicity of fluoride ions in aprotic solvents. Since our experiment was designed to eventually perform [^{18}F]fluoride labeling in aqueous solution, the use of the cryptand is not necessary.

Two different concentrations of K_2CO_3 (50 µL of 0.0774 M or 0.145 M) were tested to determine their effect on [^{18}F]F^- release efficiency. From the experimental

results tabulated in Table 3.4, the ^{18}F release efficiency observed was 82 ± 2 % for 0.0774 M, and a higher value of 93% ± 3 was found for 0.145 M of K_2CO_3. This result can be explained by considering that when a higher concentration of K_2CO_3 is used, more CO_3^{2-} is present to ion-exchange with F^-, and so a higher release efficiency is observed. Therefore, 0.145 M of K_2CO_3 was subsequently used to release $[^{18}F]F^-$ in our pre-concentration study on the MDM platform. Other releasing agents (Cs_2CO_3 and $NaClO_4$) were also used, and the release efficiency was determined (see Appendix, Section A.6).

There was a previous concern that $H[^{18}F]$ will react with the siloxane bonds on the particles. But the high release efficiency of 93% for $[^{18}F]F^-$ ions suggests that there was no significant Si-F bond formation (see Section 3.8). Also, the significant recovery of $[^{18}F]F^-$ ions captured suggests that $[^{18}F]F^-$ ions didn't react with the Teflon surface which also contains C-F bonds.

Table 3.4 Release efficiency of $[^{18}F]$fluoride ions trapped on quaternary methylammonium tagged particles using K_2CO_3 in the release solution

$[CO_3^{2-}]$	Initial Activity Captured on Particles, mCi	Activity Released, mCi	Activity left on Particles, mCi	Release Efficiency, %
0.0774 M	3.17	2.61	0.520	82 ± 2 (n=3)
0.145 M	3.50	2.64	0.795	93 ± 4 (n=5)

Small size particles (50-100 µm, 25 mg) were used. Sample calculation of release efficiency is shown on Appendix, Section A.2. All activity values are decay corrected to EOB. Operation time is 2 min and errors are SD.

3.5. $[^{18}F]$fluoride pre-concentration factor obtained on the MDM platform

For reactions discussed in Section 1.3.2, the presence of water in the reaction mixture was tolerated and good yields were still achieved. However pre-concentration of fluoride is still beneficial to increase the rate of radiochemical reactions, which typically employ small amounts of precursor in µmol or nmol quantities and in microliter volumes (Cai et al., 2008).

For all experiments, an operation time of 2 min was employed for both the capture and release steps. Since low initial activities (~2 mCi) were used, only 25 mg of magnetic particles were sufficient for capturing fluoride. For the release step, 50 µL of K_2CO_3 (0.145 M) was used. Since 1 mL of [^{18}F]fluoride/$H_2{}^{18}O$ solution was pre-concentrated to a volume of 50 µL, this gave a theoretical pre-concentration factor of 20. The pre-concentration factor was calculated using Equation 3.3. As shown on Table 3.5, the average pre-concentration factor calculated was 14.7 ± 0.3 which is considered close to the theoretical value.

Equation 3.3 Calculation of Pre-concentration factor

$$\text{Pre-concentration factor} = \%\ \text{capture} \times \%\ \text{release} \times \frac{\text{volume of } H_2{}^{18}O\ (\text{mL})}{\text{volume of released solution (mL)}}$$

Table 3.5 Pre-concentration factor calculated from capture% and release % performed on the MDM platform

Trial	% Capture	% Release	Pre-concentration factor*
1	79.29	94.54	14.99
2	78.98	94.52	14.93
3	78.47	90.87	14.26

Volume: 1 mL to 0.05 mL; Theoretical pre-concentration factor: 20-fold increase

3.6. Synthesis of [^{18}F]-labelled sulfonyl fluoride using MDM

Preparation of [^{18}F]-(2) (Scheme 1.13 in Section 1.3.2) using the conventional method was previously reported (Inkster et al., 2012). Based on their paper, [^{18}F]-(2) was synthesized in high radiochemical purity (96 ± 1 %) and it was found to have a good hydrolytic stability among other compounds studied. According to the results reported by Inkster et al. (2012), t-BuOH is the best solvent for this reaction. This conclusion is in agreement with previous reports that protic solvents, especially t-BuOH, gives a higher radiochemical yield for nucleophilic fluorination reactions, as compared to aprotic solvents such as acetonitrile (Lee, 2007; Kim 2006). The total synthesis time for this reaction was 27–31 min. The reagent volumes were in the scale of 100-200 µL and all steps were conducted manually. Considering that the method and reaction conditions

previously published can be further improved, we had chosen to do the same fluoride-exchange reaction on our MDM platform. After [^{18}F]fluoride pre-concentration was completed, the synthesis reaction was conducted on the same platform. Following the same procedure as reported by Inkster et al., a 1:1 volume ratio of the precursor (1) and [^{18}F]fluoride solution was used. However, we wanted to reduce the volume to 50 µL for both reactants. With a lower volume, we also aimed at reducing the reaction time to 5 minutes. Then, the product mixture was collected and its activity measured. Thereafter, a 40 µL aliquot was taken for HPLC analysis.

Figure 3.5 shows the HPLC chromatogram of the product mixture using both the UV-absorbance and radioactive detectors. Reference standard, [^{19}F]-(2) was previously analyzed on HPLC and the retention time was found to be 10.9 min by UV detection (Figure 3.5A upper trace). This retention time was compared to the retention time of [^{18}F]-(2) to confirm the identity of the radioactive product formed, as shown in Figure 3.5B. Considering that the injected sample is first read by the UV detector, followed by the radioactive detector, the peak for [^{18}F]-(2) was expected to appear with a delay of approximately 0.2 min in the radioactive chromatogram. Thus the times of 10.9 min from UV detection and of 11.1 min from radioactive detection represents the retention times of [^{19}F]-(2) and [^{18}F]-(2), respectively. The upper red line on Figure 3.5A represents the product mixture which was spiked with the [^{19}F]-(2) and the bottom blue line (without spiking) was used to calculate specific activity. The specific activity was calculated as shown in Appendix, Section A.5. The apparent specific activity of [^{18}F]-(2) prepared in this fashion was estimated to be 48 ± 3 GBq/µmol (1.3 Ci/µmol) at n=3 based on the UV-HPLC signal and the radioactive signal. A value of 18.5 GBq/µmol (0.5 Ci/ µmol) is generally considered as the minimum activity required for PET imaging (Jacobson et al., 2011) and a value of 37–74 GBq/µmol (1–2 Ci/ µmol), is commonly described as ‘high’ for PET imaging (Cai et al., 2008).

Nevertheless, our specific activity obtained was lower compared to 105 GBq/µmol (2.8 Ci/µmol) that was reported by Inkster et al. This difference may be attributed to the low initial activities (2-5 mCi) that we used as compared to the activities used by Inkster et al. (>5-10 mCi). It has been previously observed that when the initial activity used is lower, the specific activity of the product will be lower (Liu et al., 2012).

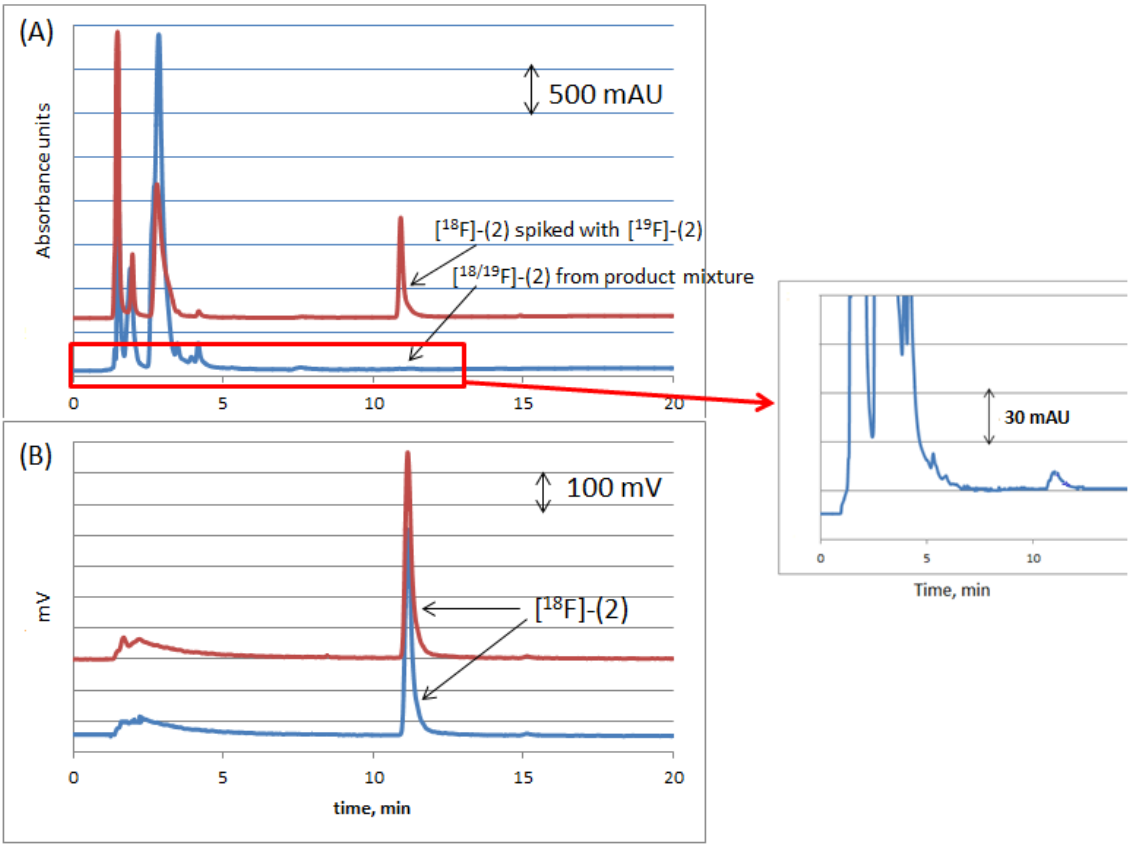

Figure 3.5 (A) UV detection (254 nm) of the product mixture. The inset shows the expanded region around 10 min. (B) Radioactive detection showing the presence of [^{18}F]-(2) in the same product mixture.

Note: Red line shows the product mixture spiked with reference standard, [^{19}F]-(2) and the blue line shows product mixture without spiking. HPLC conditions: Isocratic flow = 1.00 mL/min, 30:70 MeCN:H_2O.

The peaks eluted between 2-5 minutes may be caused by impurities in the product mixture. Therefore, control experiments have been performed in the product mixture in order to find out the source of these peaks. As shown in Figure 3.6 (line a), peaks at 2-3 min, though of smaller peak heights, were already present in the [^{18}F]fluoride solution obtained from the cyclotron. Similar peaks were also observed after the [^{18}F]fluoride solution was pre-concentrated in MDM, before the synthetic reaction (Figure 3.6, line b). Since the similar peaks were present before and after the treatment with the particles, we can say that these peaks do not come from any possible impurities in magnetic particles or on the Teflon surface. These small peaks could be the fluoride ions in the solution. When the [^{18}F]fluoride solution was allowed to react with the

precursor (1), the product, [^{18}F]-(2) was formed along with the impurities peaks which are now larger in size (Figure 3.6, line c). These larger peaks were observed even when ^{19}F solution was used to synthesize [^{19}F]-(2) (Figure 3.6, line d). From Figure 3.6, line e, we confirmed that aside from the peaks due to the precursor (1) and [^{19}F]-(2), peaks due to the tBuOH solvent also appeared in ~3 minutes.

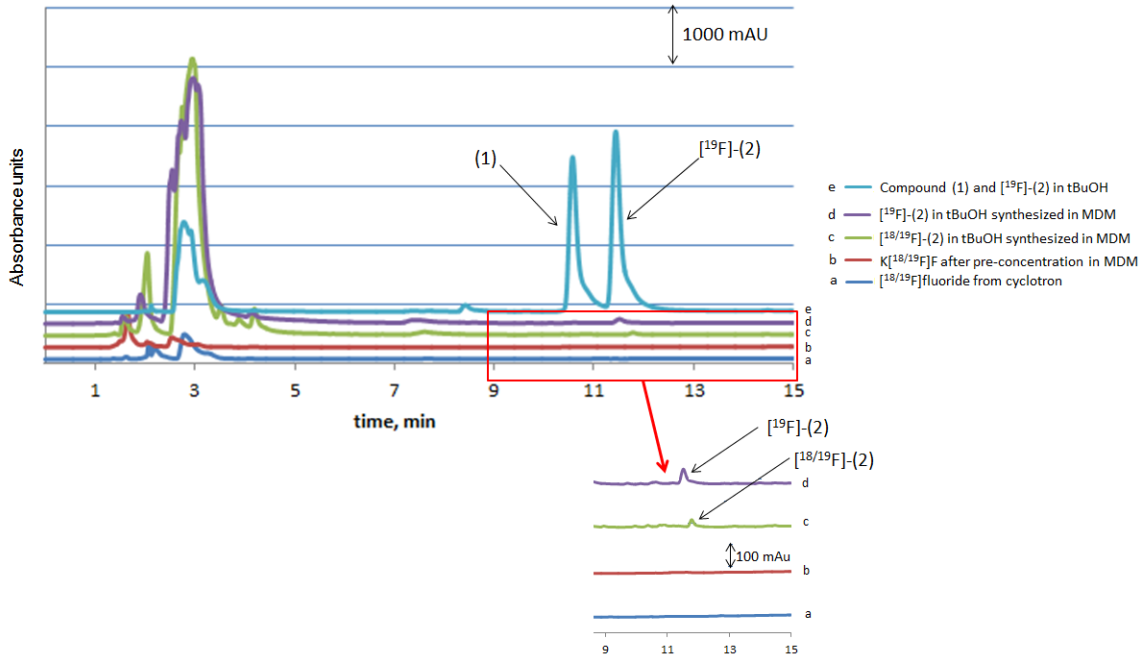

Figure 3.6 Control experiments to reveal the source of peaks eluted at 2-5 minutes

Note: (a) These peaks were already present in the [^{18}F]fluoride solution obtained from the cyclotron (b) Same peaks were observed after the [^{18}F]fluoride solution was pre-concentrated in MDM (c) The same peaks were observed after the pre-concentrated [^{18}F]fluoride was allowed to react with precursor (1) to form product, [^{18}F]-(2) (d) The same peaks were observed when using [^{19}F]fluoride to form [^{19}F]-(2) (e) A solution of (1) and [^{19}F]-(2) in tBuOH was injected in HPLC, showing peaks at 2-5 min. The inset diagram shows the expanded region at around 11 min. HPLC injection volume for all experiments is 50 µL.

To summarize the results of these control experiments, it was found that peaks eluted at 2-5 minutes shown in the chromatogram (Figure 3.6) were contributed by the fluoride and/or the tBuOH solvent used. Some of these impurity peaks can be removed by passing the product mixture through a SPE column prior to HPLC injection, see Figure 3.7.

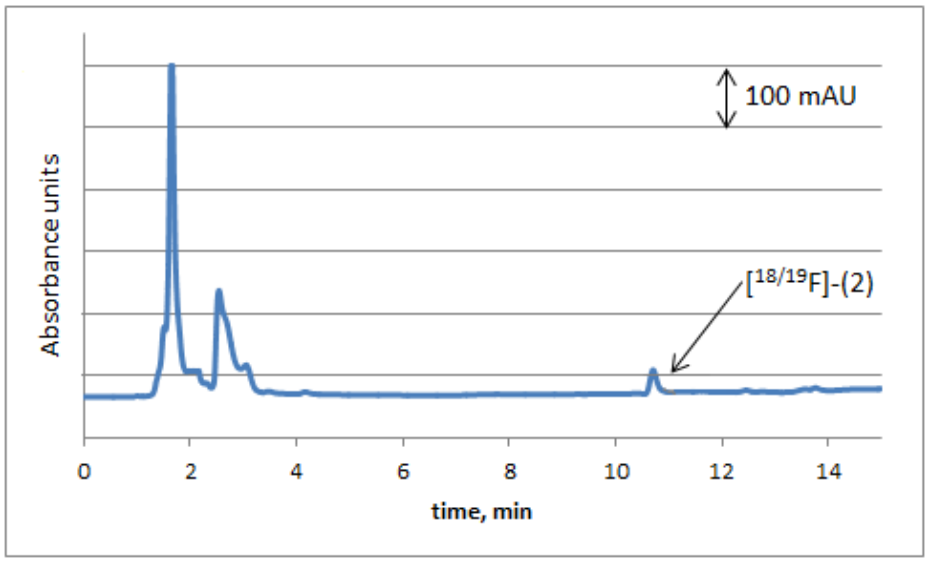

Figure 3.7 HPLC result of the product mixture of [$^{18/19}$F]-(2) after SPE purification. UV detection at 254 nm.

The results for the synthesis of [^{18}F]-(2) are tabulated in Table 3.6. A radiochemical purity of 90-95% was obtained from the HPLC peak area % using Equation 3.4. The radiochemical yield is calculated based on the activity of the isolated product against initial radioactivity using Equation 3.5 and the values calculated are 62-72%.

Equation 3.4 Calculation of Radiochemical Purity

$$\text{Radiochemical Purity of (2)} = \frac{\text{RAD-HPLC peak area of (2)}}{\text{Total RAD-HPLC peak areas}} \times 100\%$$

Equation 3.5 Calculation of Radiochemical Yield

$$\text{Radiochemical Yield (RCY)} = \frac{\text{Total radioactivity recovered x Radiochemical Purity}}{\text{Initial Radioactivity Used}} \times 100\%$$

Table 3.6 Results for the synthesis of [^{18}F]-(2)

Capture %	Release %	Volume of Precursor [1], 0.06 M	Radiochemical Purity, %	Radiochemical Yield (RCY), %
78 ± 3	94 ± 3	50 µL	90±1	62±5
		60 µL	95±1	72±1

Sample calculation of Radiochemical yield is shown in Appendix, Section A.4. Activities are decay-corrected to EOB and errors are SD (n=3).

It was found that an increase in the volume of precursor (1) used, increases the amount of the product formed. This increase leads to an improvement of the radiochemical purity from 90% to 95% thereby increasing the RCY value to 72%. It was observed that although the release % was quite high, the low capture % has resulted in a low RCY. We believe that this low capture % is caused by the saturation of the quaternary ammonium binding sites in the magnetic particle surface. This issue could be resolved by using more magnetic particles and in smaller sizes, as discussed in section 3.4.

We compared our results with those obtained from the conventional method (Inkster et al., 2012) and from the Advion Nanotek Microfluidic System (Matestic et al., 2013), see Table 3.7. The radiochemical purity of 96% and RCYs of 72% obtained from our MDM method are comparable with those values obtained from the other two methods. Moreover, the automated process performed on the MDM platform is an attractive feature because of reduced operator radiation exposure and less contribution of human error, resulting in better results. Similar to most microfluidic systems, our MDM platform offers the advantage of dealing with small volumes of reagents and precursors.

With the work published by Matestic et al., only the mixing of ^{18}F and precursor took place in the microreactor. But the pre-concentration step was still conducted on a conventional quaternary methylammonium (QMA) anion-exchange column. In our case, we demonstrated that both pre-concentration and synthesis could be conducted on the same platform. The drying method after [^{18}F]fluoride pre-concentration was eliminated and the total synthesis time was reduced to ~15 min. Moreover, the use of K222-cryptand is eliminated and only K_2CO_3 solution is used as the releasing solution. Our

MDM method offers a simpler and safer approach leading to an easier module development for the preparation of ^{18}F radiotracers.

With our pre-concentration method, [^{18}F]fluoride was released from the particles in a smaller volume (50 µL) as compared to 200-250 µL which is currently being used in conventional methods (using the QMA trap and release column). Even when performed in low volumes, we were still able to produce [^{18}F]-(2) at high radiochemical purity (95%).

Table 3.7 Method comparison for the synthesis of [^{18}F]-(2)

	^{18}F Solution	**Precursor (1)**	**Pre-concentration time**	**Reaction time**	**Radiochem Purity,%**	**RCY %**
Conventional (Inkster et al.)	5-10 mCi 100-200 µL	0.060 M 100 µL	5 min.	15 min.	96±1	73±7
Advion Nanotek (Matestic et al.)	0.27-0.40 mCi 10 µL	0.0081 M 10 µL	20-30 min. with drying step	2 min.	97	75
Magnetic Droplet Microfluidics (MDM)	2-6 mCi 50 µL	0.060 M 50-60 µL	5 min.	5 min.	96±1 (n=3)	72±1 (n=3)

3.7. Synthesis of rhodamine-^{18}F-$ArBF_3$ (5)

The MDM method provides a unique opportunity to develop other types of ^{18}F-labeling radiochemistry. For proof of concept, the MDM method has been applied to another ^{18}F chemistry such as the [^{18}F]$ArBF_3$ chemistry developed by Perrin group at UBC.

As mentioned in Section 1.3.2, reactions of [^{18}F]F^- with boron to form aryltri-[^{18}F]fluoroborates have been reported by Liu et al. (2012). In that report, the authors successfully demonstrated the isotope exchange reaction of $^{19}F^-$ with $^{18}F^-$ to form an ^{18}F-labelled $ArBF_3$ compound. In their other paper (Liu et al., 2013), they further attached the labeled $ArBF_3$ to an RGD peptide to produce a clinically useful radiotracer for PET

imaging. High specific activity of the radiotracer along with its rapid clearance in vivo was achieved.

In our experiment, the same isotope exchange reaction was performed using the fluorescent rhodamine-[^{19}F]-$ArBF_3$ precursor (see Scheme 1.11 in Section 1.3.2). The synthesis of this compound was performed as previously described in Liu et al. (2012). We used the reported method and reaction conditions to synthesize [^{18}F]-(5), with the exception that very low activities were used (4-5 mCi). Using the low activity of [^{18}F]fluoride, we can directly compare our MDM results with the results obtained with their method.

Since low activities were used in our study, the addition of KHF_2 was necessary in order to increase the amount of F^- ions in the solution. This is because a relatively high concentration of aqueous fluoride is required to facilitate the ion-exchange reaction. At least 3 equivalents of fluoride are required to convert each arylboronic ester to $ArBF_3^-$ as shown in Scheme 3.5 (Ting et al., 2008). Moreover, sodium perchlorate ($NaClO_4$), instead of K_2CO_3, was used as the releasing solution since it is important that the pH value was maintained at 2 for the synthesis reaction to occur. Arylboronic ester has to be converted back to the $ArBF_3^-$ and this reaction is enhanced at low pH where solution acidity protonates the RO group (in the arylboronic ester) to facilitate its displacement by fluoride.

$$ArB(OR)_2 + KF + 2HF \rightleftharpoons ArBF_3K + 2ROH$$

Scheme 3.5 Formation of $ArBF_3K$ from $ArB(OR)_2$

Based on the results reported by Liu et al. (2012), the use of >800 mCi activity gave an RCY of 40–50%. In their case, high activities were used and so the addition of KHF_2 was not necessary. In our experiment using the conventional method, 4-5 mCi of [^{18}F]fluoride and the addition of 17.5 nmol KHF_2 only gave a radiochemical purity of 6.0% (Table 3.8). An experiment was also performed wherein no KHF_2 was added, but when the reaction mixture was analyzed on HPLC, no product was formed. Higher activities of [^{18}F]fluoride were not used due to safety issues and due to the limited amount of precursor (4).

Table 3.8 Synthesis of [^{18}F]-(5) by the conventional method

Activity used for the reaction	4.50 mCi (~30 µL)
Precursor (compound [4])	50 nmol in 20 µL
Pyridazine-HCl Buffer (pH 2)	10 µL
KHF_2 added	17.5 nmol in 1 µL
Temperature	40°C
Reaction time	10-15 minutes
Radiochemical Purity of compound [5] by HPLC	6.0% ± 0.3 (n=2)

The synthesis of [^{18}F]-(5), with the pre-concentration step, was then conducted on MDM platform. Initial activities of 4-5 mCi of [^{18}F]fluoride were also used. The steps described in Figure 2.5 were followed except that after the pre-concentration step the NR_4^+-tagged magnetic particles came in contact with the pH 2 solution to create a stirring motion within the droplet. This experiment has been performed at room temperature, which is labeled as "**Experiment A**", and the reaction conditions and results are listed in Table 3.9. From HPLC analysis, a low radiochemical purity of 1.1% had resulted. One reason for the low purity could be that this experiment was conducted at room temperature rather than at 40°C.

Another reason for the low product purity is that the Si-O-Si (siloxane) bonds on the magnetic particles may be attacked by [^{18}F]fluoride, forming stable Si-F bonds. One possible mechanism for HF reaction with the siloxane bond is shown in Scheme 3.6 (Knotter, 2009). If this side-reaction occurs, a siloxane bond would be broken but the silica moiety might still remain on the particle surface. However, the fluoride attached to Si is not capable of ion-exchange reaction, resulting in an apparent increase in capture but certainly a decrease in the F^- release efficiency.

One must note that the breaking of the siloxane bond occurs in the presence of HF. It was previously reported that there is a linear relationship between the dissolution rate of the siloxane bonds and the concentration of HF_2^- and HF. Thus, the rate of the breaking of the siloxane bonds increases when the pH of the solution is lower (Judge, 1971; Gaines, 2014).

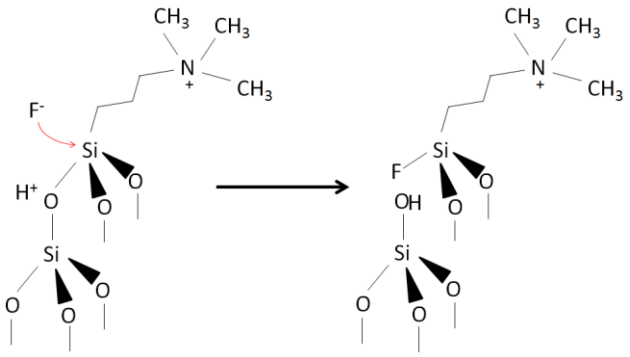

Scheme 3.6 Proposed nucleophilic substitution reaction for breaking of the siloxane bond by HF

The [^{18}F]fluoride solution produced from TR-13 cyclotron is only weakly acidic with a measured pH of around 5.5. Thus, one can expect that the formation of Si-F would be less significant than when the pH is lower. We verified the low extent of formation of Si-F bond by conducting a fluoride capture experiment using non-modified silica-coated particles at pH 5.5. The particles were first allowed to react with [^{18}F]fluoride solution coming from the cyclotron. It was observed that only 2.6 ± 0.5 % of [^{18}F]F^- ions were captured by the non-modified silica-coated particles. As one can recall, QMA-tagged magnetic particles were able to capture 59-93% of $^{18}F^-$ (see Table 3.2). The low value of 2.6% compared to 59-93% capture efficiency explains that almost all of the F^- ions are not captured if the silica-coated particles are used. The QMA ion has to be present on the surface of the particle to achieve high capture efficiency and these fluoride ions are releasable by an ion-exchange reaction.

Another experiment was conducted at low pH where silica-coated particles were allowed to react with [^{18}F]fluoride solution in the pH 2 buffer (pyridazine-HCl). This pH 2 buffer is used to make the same acidity as required in the synthesis of [^{18}F]-(5). With the higher acidity, the HF concentration is also increased. The initial activity of [^{18}F]fluoride as well as the activity on the waste and the activity left on the non-modified silica-coated particles were measured and shown in a histogram in Figure 3.8.

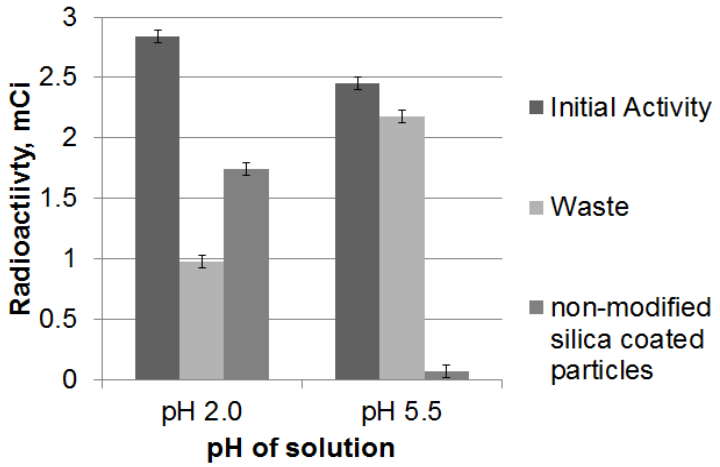

Figure 3.8 The extent of HF-mediated hydrolysis on the non-modified silica-coated particles at two pH values

Note: On the experiment at pH 5.5, the [^{18}F]fluoride solution produced from the cyclotron was directly used. On another experiment, this [^{18}F]fluoride solution was added with a pH 2.0 pyridazine-HCl buffer solution. The activities of the [^{18}F]F$^-$ ions captured on the particles and the ions remained in the waste were measured and the decay-corrected values were shown.

Non-modified silica-coated particles captured an average of 2.6% of [^{18}F]F$^-$ ions at pH 5.5 and a high activity remained in the "waste". These values are compared to an unusually high 57.7% of [^{18}F]F$^-$ ions "captured" at pH 2. Thus, the slightly acidic nature of [^{18}F]fluoride solution produced from the cyclotron would not cause cleavage of the siloxane bonds as long as the pH of the reactant solution is not made too low subsequently.

To avoid the detrimental effect of the pH 2 buffer used in the radiosynthesis reaction for [^{18}F]-(5) on the QMA magnetic particles, they were removed out of the platform after the pre-concentration step was completed. To achieve this removal, the particles on the Teflon surface were moved toward a barrier which stopped the particles in a certain area, see Figure 2.5. The robotic arm then picked up a bare carrier magnet to stir the reaction mixture. Moreover, the temperature on the platform was increased (maintained at 40^{o}C) by using a heating lamp as shown in Figure 2.4. This higher-temperature experiment is labelled as "**Experiment B**" and the reaction conditions and results are tabulated in Table 3.9. As compared to Experiment A, a higher radiochemical purity was achieved (5.8%). This is because the release efficiency was increased from 17% to 58%, and also the reaction temperature was increased to 40^{o}C in Experiment B.

Figure 3.9 shows the HPLC chromatogram of a product sample obtained in Experiment B. The RAD-HPLC shows two peaks: peak 1 corresponds to unreacted [^{18}F]fluoride (~3.0 min) and peak 2 corresponds to the desired [^{18}F]-(5) (~11.1 min). In the UV-HPLC result, three peaks appear: peak 3 corresponds to the rhodamine isomer which is present as an impurity when rhodamine was purchased; peak 4 corresponds to the product, [$^{18/19}$F]-(5); and peak 5 corresponds to the arylboronic ester.

When a low [^{18}F]fluoride activity (4-5 mCi) was used, the radiochemical purity obtained in the MDM method is 5.8% which is comparable to the value of 6.0% obtained using the conventional method (see Table 3.9). These values obtained from the MDM are not yet optimized and there are still a lot of factors to be studied and improved in the future. Nevertheless, here we are able to demonstrate that the MDM platform can be used to perform another type of ^{18}F-labeling reaction.

Table 3.9 Synthesis of [^{18}F]-(5) in MDM

	Experiment A	**Experiment B**
Mass of Magnetic Particles	~40 mg	~40 mg
Initial Activity of ^{18}F	31.5 mCi	33.9 mCi
Capture %	58.5%	48.2%
Release %	15.2%	57.0%
Activity after pre-concentration	2.80 mCi in 50 µL	9.32 mCi in 50 µL
Precursor	50 nmol in 50 µL	50 nmol in 50 µL
Volume of Buffer (pH 2)	10 µL	10 µL
KHF_2 added	17.5 nmol in 1 µL	17.5 nmol in 1 µL
Temperature	Room temperature	40°C
Reaction Time	10-15 min	10-15 min
Radiochemical Purity	1.1%	5.8%

Note: In Experiment A, the QMA-modified magnetic particles had come in contact with the pH 2 solution while this is not the case for Experiment B (only a bare magnetic carrier was used for stirring). All activities are decay-corrected to EOB.

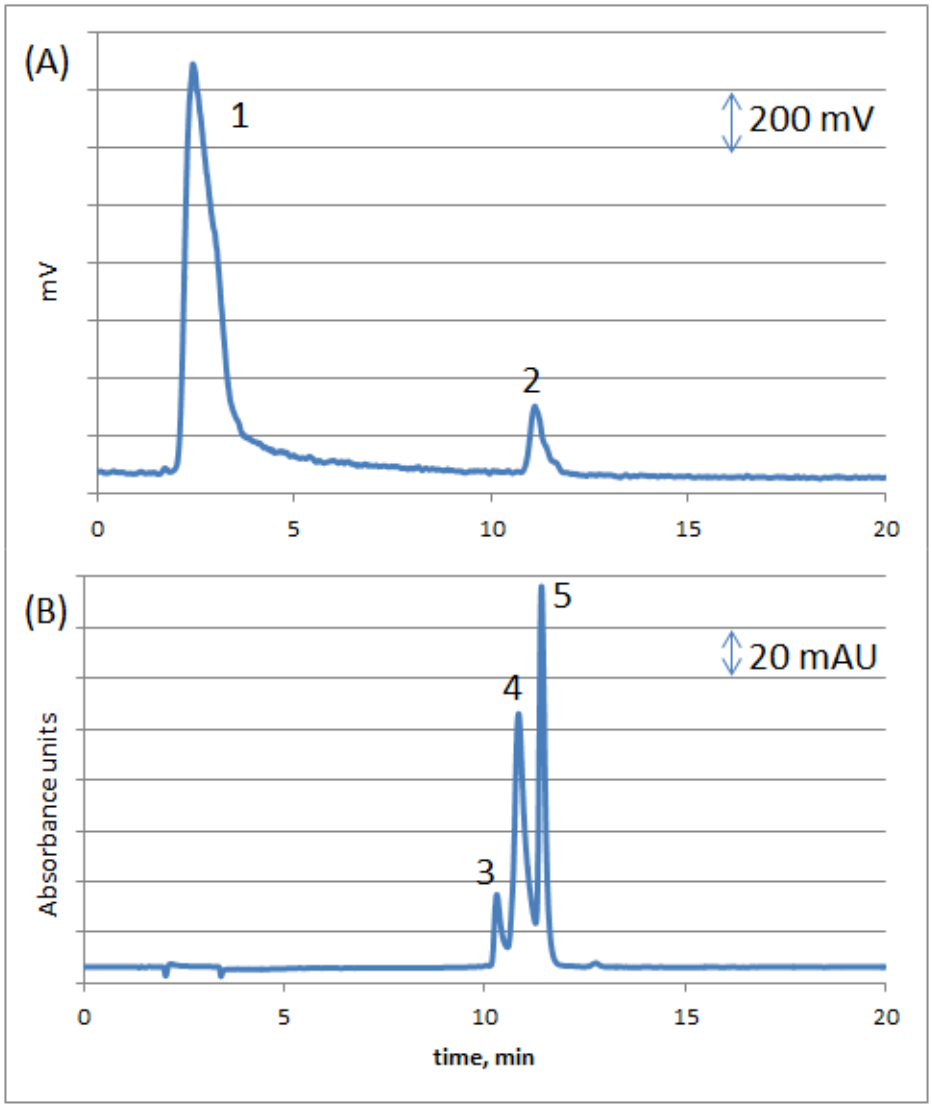

Figure 3.9 **HPLC analysis of [^{18}F]-(5) synthesized using the MDM method. (A). RAD-HPLC (mV); (B) UV-HPLC (mAU) (540 nm). Isocratic flow = 1.10 mL/min, 30:70 MeCN: H_2O.**

Chapter 4. **Conclusion and Future Work**

4.1. Conclusion

Herein, we showed that the synthesized QMA-tagged magnetic particles can be used to capture [^{18}F]fluoride ions in a solution and the captured [^{18}F]fluoride ions are released by ion-exchanging with a K_2CO_3 solution. The new MDM platform was also developed as a safe and simple alternative method to carry out radiochemical reactions in microliter volumes.

In terms of the capture efficiency of the magnetic particles, it was found that as the activity was increased (thereby increasing the mass of fluoride ions), the capture efficiency decreased since the ion-exchange sites in the particles are fully occupied or saturated. Thus, it is expected that as the size of the particles is decreased, the surface area is increased leading to more ion-exchange sites. It was observed that the particles with smaller sizes (50-100 µm) had captured more fluoride ions. The highest capture efficiency achieved when using 25 mg of particles was 79 ± 3% at initial activities of ~2 mCi, and that was only 35 ± 3 % at initial activities of ~30 mCi. However, when the mass of magnetic particles was increased to 40 mg, a capture efficiency of 51 ± 3% was achieved at initial activity of 32 mCi. On the other hand, the releasing efficiency achieved was 93 ± 3 %.

By using the MDM platform to carry out the liquid droplet manipulation, the pre-concentration step took approximately 5 min. and the [^{18}F]fluoride solution was pre-concentrated by 15-fold from a liquid volume of 1 mL to 0.05 mL. A small volume of 0.05 mL was achieved without the need of a drying step as required in conventional method. Pre-concentration is necessary even with aqueous ^{18}F chemistry to reduce the volume of [^{18}F]fluoride solution (thereby increasing the fluoride concentration) since radiochemical reactions typically employ small amounts of precursor in umol or nmol quantities and in microliter volumes (Cai et al., 2008).

After the pre-concentration step, an ^{18}F-labelling reaction was performed on the MDM platform based on the S-F bond formation to produce an arylsulfonyl [^{18}F]fluoride which can be used as a prosthetic group to label PET targeting ligands. The high radiochemical purity of 95 ± 1% was comparable with 96% which was previously reported using conventional method. Similarly, radiochemical yields (RCYs) of ~70% were also comparable at initial activity of ~2 mCi. However, the total synthesis time was improved to ~15 minutes with the use of lower reagent volumes (50-60 µL). Furthermore, radiation exposure was minimized since the MDM method was automated and the operation was performed by a computer located outside the hotcell.

The MDM method was also used to produce an ^{18}F-labelled aryltrifluoroborate through B-F bond formation. Since low initial activities (~5 mCi) were used, the radiochemical purities achieved were low for both the MDM method (5.8 %) and the conventional method (6.0 %). These RCY values obtained from the MDM method were not yet optimized. Nevertheless, we are able to provide a proof of concept that the MDM method can be used to perform another type of ^{18}F-labeling reaction and can be used in the future to produce an ^{18}F-labelled peptide-ArBF_3.

In the light of developing novel concepts for conducting ^{18}F radiochemistry, this thesis introduces the use of a novel microfluidic design as a potential method for the routine production of ^{18}F radiotracers. When the MDM platform is used, the pre-concentration and synthesis steps can be integrated on the same platform while using microliter volumes of reagents. This automated process also offers the advantage of reduced production time and volume, minimal operator radiation exposure, and facile operation outside the hot cell.

4.2. Future work

4.2.1. Design of the MDM platform

In order for the MDM platform to be used for radiochemical synthesis, the platform should be miniaturized to reduce the space required for the apparatus in hot cells. Currently, the whole MDM set-up occupies approximately 24” by 15” of space inside the hot cell including the X-Y plotter, stage, heating lamp, iron stands and 2 syringe pumps. The equipment that takes much of the space and should be miniaturized is the X-Y plotter (15” x 12”) and the syringe pumps (10” x 4”). Furthermore, a permanent cover should be placed on the Teflon platform in order to prevent the reaction reagents from being exposed to moisture and to prevent evaporation. Depending on the project budget, we believe that these equipment issues can be easily addressed by smart engineering designs to build a more compact and flexible MDM prototype.

4.2.2. Synthesis and Characterization of Magnetic Particles

The number of ion-exchanging sites in the particles can be characterized in detail. First, the nitrogen content of the aminated silica surface can be determined by the Kjeldahl method. This method has been used previously (Campos et al., 2001) to determine the number of moles of nitrogen on a silica surface. The number of moles of iodide on the particle surface can also be determined. This can be achieved by reacting the QMA iodide-functionalized particles with a sodium chloride solution so that the iodide ion will be replaced with chloride through an ion-exchange reaction. The chloride ion present on the particles will then be determined by potentiometric titration with a $AgNO_3$ standard solution (Campos et al., 2001). The value calculated for chloride is equivalent to the iodide ion available on the particle surface. Infrared spectra of the unmodified particles and QMA-functionalized particles can also be obtained to determine whether amine and methyl groups are present. After an in-depth characterization of the ion-exchanging sites on the particle surface, the procedure for functionalizing the particles can then be optimized by changing the amount of reagents used and varying other reaction conditions. Production of smaller sizes of particles (< 50 µm) can also be further explored to increase the particle surface area, and hence the ion-exchanging sites.

4.2.3. Radiochemical synthesis on the MDM platform

The ^{18}F-labeling reactions performed in this thesis work were designed in order to synthesize ^{18}F radiotracers which can be used for PET imaging. As a proof of principle, the sulfonyl [^{18}F]fluoride prosthetic group, [^{18}F]-(2) will then be attached to a PET targeting peptide to finally produce an end product which can be used for imaging. For example, [^{18}F]-(2) can be attached to a bombesin peptide by an oxime linkage (Inkster et al, 2012). This additional step can also be performed on the same MDM platform.

For aryl[^{18}F]trifluoroborates such as [^{18}F]-(5), a one-step labeling reaction will be performed wherein a biotin-linked $ArBF_3$ (Ting et al, 2008) or a peptide-linked $ArBF_3$ such as RGD-$ArBF_3$ (Liu et al., 2013) is used to directly react with the pre-concentrated [^{18}F]fluoride on MDM. An ^{18}F-labelled biotin-$ArBF_3$ or RGD-$ArBF_3$ can then be used for PET imaging.

4.2.4. Integration of Purification Step on MDM method

Strategies can be explored in order to incorporate the purification step on the MDM platform. For example, it has been reported that biotin and nitroavidin will bind strongly to each other at pH 4 to 7 but there is no binding at pH 10 (Morag et al, 1996). If a biotin-ArB[^{18}F][^{19}F]$_2$ is synthesized, a nitroavidin-functionalized magnetic particle can be used to capture both the biotin-$ArBF_3$ (unreacted precursor) and biotin-ArB[^{18}F][^{19}F]$_2$ (product) at pH 4-7. This will separate the product from any unreacted free fluoride which has to be removed since free fluoride ions are toxic to the human bone. At pH 10, both biotin-$ArBF_3$ and biotin-ArB[^{18}F][^{19}F]$_2$ can then be released out from the particle and then collected into a vial. These steps can be manipulated on the MDM platform since magnetic particles are used. Similar strategies can also be explored for peptide-linked prosthetic compounds.

References

Abu-much, R., et al., Formation of a Three-Dimensional Microstructure of Fe_3O_4 Poly(vinyl alcohol) Composite by Evaporating the Hydrosol under a Magnetic Field. *J. Phys. Chem*. B, 2006. 110: p. 8194-8203.

Advion [accessed 2014]; Available from: http://www.advion.com/biosystems/nanotek/nanotek-positron-emission-tomography-references.php.

Ametamey, S.M., et al., Molecular Imaging with PET. *Chem Rev*., 2008. 108 (9): p. 4036.

Asti, M., et al., Purification by ozonolysis of 18O enriched water after cyclotron irradiation and the utilization of the purified water for the production of [18F]-FDG (2-deoxy-2-[18F]-fluoro-Dglucose). *Appl. Radiat. Isot*., 2007. 65: p. 831-835.

Balaban, A.T., et al., Labelled compounds and Radiopharmaceuticals Applied in Nuclear Medicine. John Wiley and Sons, New York, 1986.

Barrio, J.R., et al., Remote, semiautomated production of [18F]-labeled 2-deoxy-2-fluoro-D-glucose. *J. Nucl. Med*., 1981. 22: p. 372-375.

Baudot, P., et al., Effect of diaza-polyoxa-macrobicyclic complexing agent on the urinary elimination of lead in lead-poisoned rats. *Toxicol. Appl. Pharmacol.*, 1977. 41: p. 113 – 118.

Bendriem, B. and D.W. Townsend (Eds.), The theory and practice of 3D PET (Developments in Nuclear medicine), Kluwer, Dordrecht, Netherlands, 2008.

Bergstrom, M., et al., Positron emission tomography microdosing: a new concept with application in tracer and early clinical drug development. *Eur. J. Clin. Pharmacol.*, 2003. 59: p. 357-366.

Beringer, R. and C.G. Montgomery, The angular distribution of positron annihilation radiation. *Phys. Rev.*, 1943. 61: p. 222-224.

Block, D., et al., The N.C.A. nucleophilic 18F-fluorination of1,N-disubstituted alkanes as fluoroalkylation agents. *J. Labelled Compd. Radiopharm.*, 1987. 24: p. 1029-1042.

Blower, P. (2006) Towards molecular imaging and treatment of disease with radionuclides: the role of inorganic chemistry. *Dalton Trans.* 1705–1711.

Bouvet, V.R., et al., Synthesis of hypoxia imaging agent 1-(5-deoxy-5-fluoro-α-D-arabinofuranosyl)-2-nitroimidazole using microfluidic technology. *Nucl. Med. Biol.*, 2010. 38(2): p. 235.

Brink, J., PET/CT Unplugged: The Merging Technologies of PET and CT Imaging. *American J Roentgenol*, 2005. 184: S135-S137.

Brodack, J.W., et al., Robotic production of 2-deoxy-2-[18F]fluoro-D-glucose: A routine method of synthesis using tetrabutylammonium [18F]fluoride. Int. J. Radiat Appl. Instrumen. Part A. *Appl. Radiat. Isot.*, 1988. 39: p. 699-703.

Bruce, I.J., et al., Synthesis, characterisation and application of silica-magnetite nanocomposites. *Journal of Magnetism and Magnetic Materials*, 2004. 284: p. 145–160.

Burger, C., et al., PET attenuation coefficients from CT images: experimental evaluation of the transformation of CT into PET 511-keV attenuation coefficients. *Eur. J. Nucl. Med. Mol. Imag.* 2002. 29: p. 922-927.

Cai, L.S., et al., Chemistry with [18F]fluoride ion. *Eur. J. Org. Chem*, 2008.17: p. 2853-2873.

Campos, E., et al., Quaternary ammonium salts immobilized on silica gel: exchange properties and application as potentiometric sensor for perchlorate ions. *Journal of Colloid and Interface Science*, 2001. 240: p. 97-104.

Chun, J.-H., et al., Fast and High-yield Micro-reactor Syntheses of Ortho-substituted [^{18}F]Fluoroarenes from Reactions of [^{18}F]Fluoride Ion with Diaryliodonium Salts. *J. Org. Chem.*, 2010. 75(10): p. 3332.

Clark, J.H., Fluoride ion as a base in organic synthesis. *Chem. Rev.*,1980. 80, p. 429-452.

Coenen, H.H. in PET chemistry: the Driving Force in Molecular Imaging (Eds.: P. A. Schubiger, L. Lehmann, M. Friebe), Springer, Heidelberg, 2007, p. 15 –36.

Day, P., et al. (eds.), Microdroplet Technology: Principles and Emerging Applications in Biology and Chemistry, Integrated Analytical Systems, Springer Science-Business Media, LLC, 2012.

De Leonardis, F., et al., On-chip pre-concentration and complexation of [18F]fluoride ions via regenerable anion exchange particles for radiochemical synthesis of Positron Emission Tomography tracers. *Journal of Chromatography A*, 2011. 1218: p. 4714– 4719.

De Leonardis, F., Microfluidic modules for pre-concentration of [^{18}F]fluoride in positron emission tomography (PET) radiotracer synthesis (Doctoral Thesis Dissertation). The University of Hull, United Kingdom, 2012.

Dorvee J, et al., Manipulation of liquid droplets using amphiphilic, magnetic one-dimensional photonic crystal chaperones. *Nat Mater*, 2004. 3: p. 896–899.

Duffin, W.J., Electricity and Magnetism. 4th ed., McGraw-Hill Book Company Europe, Maidenhead, UK, 1990.

Fowler, J.S., et al., A shielded synthesis system for production of 2-deoxy-2-[18F]fluoro-D-glucose. *J. Nucl. Med.*,1981. 22: p. 376-380.

Futchner, F., et al., Factors affecting specific activity of [18F]fluoride from [18O]water target. *Nuklear Medizin*, 2008. 47 (3): p. 116-9.

Gaines, P., [accessed Oct 2014] Compatibility and Precision Issues: ICP Operations Guide: Part 6. Available from: http://www.inorganicventures.com/compatibility-and-precision-issues.

Gijs, M.A.M., Magnetic bead handling on-chip: new opportunities for analytical applications. *Microfluid. Nanofluid.*, 2004. 1(1): p. 22.

Gijs, M.A.M., et al., Microfluidic applications of magnetic particles for biological analysis and catalysis. *Chem. Rev.*, 2010. 110(3): p. 1518.

Gillies, J.M., et al., Microfluidic technology for PET chemistry. *Appl. Radiat. Isot.*, 2006. 64(3): p. 333.

Graham, T.J.A., et al., Enantioselective Radiosynthesis of Positron Emission Tomography (PET) Tracers containing [^{18}F]Fluorohydrins. *J. Am. Chem. Soc.*, 2014. 136: p. 5291-5294.

Gushikem, Y. and J.C. Moreira, Adsorption of MX_2 (M = Mn, Ni, Cu, Zn, and Cd; X = Cl, Br, and I) and $FeCl_3$ by modified silica surface with imidazolylpropyl group. *J. Colloid Interface Sci.*, 1985. 107 (1): p. 70-74.

Hamilton, L.V., Oak Ridge Reservation Annual Site Environmental Report for 1996. 1997.

Hamacher, K., et al., Efficient stereospecific synthesis of nocarrier-added 2-[18F]-fluoro-2-deoxy-D-glucose using aminopolyether supported nucleophilic substitution. *J. Nucl. Med.*, 1986. 27: p. 235-238.

Haroun, S., et al., “Continuous-flow synthesis of [11C]raclopride, a PET radiotracer, on a microfluidic chip”, *Can. J Chem.*, 2013. 91: p. 326-332.

Henriksen, G., et al., A fully automated “In-capillary reaction” platform. EANM Pre-congress symposium on Microfluidic Production of Radiopharmaceuticals, Germany, 2008.

Hess, E., et al., Improved target system for production of high purity [18F]fluorine via the 18O(p,n)18F reaction. *Appl Radiat Isotopes*, 2000. 52: p. 1431-1440.

Holleman, A. F. and E. Wiberg, Inorganic Chemistry. Academic Press, San Diego, 2001.

Huang, X., et al., Late Stage Benzylic C-H Fluorination with [^{18}F]Fluoride for PET Imaging. *J. Am. Chem. Soc.*, 2014.136: p. 6842-6845.

IAEA, Cyclotron Produced Radionuclides: Physical Characteristics and Production Methods. International Atomic Energy Agency, 2009. www.pub.iaea.org/MTCD/publications/PDF/trs468_web.pdf.

Inkster, J. A. H., et al., Sulfonyl fluoride-based prosthetic compounds as potential ^{18}F labeling agents. *Chem. Eur. J.*, 2012. 18: p. 11079-11087.

Jacobson, O., et al., Rapid and simple one-step labeling of peptides. *Bioconj. Chem.*, 2011. 22: p. 422.

Judge, J.S., A study of the dissolution of SiO_2 in acidic fluoride solutions. *J Electrochem. Soc.*, 1971. 118 (11): p. 1772-1775.

Laali, V.J., et al., Fluorodediazonization in ionic liquid solvents: new life for the Balz-Schiemann reaction. *J. Fluorine Chem.,* 2001. 107: p. 31-34.

Laverman, P., et al., A novel facile method of labeling octreotide with 18F-fluorine. *J Nucl Med,* 2010. 51: p. 454-461.

Le Bars, D., Fluorine-18 and medical imaging: Radiopharmaceuticals for positron emission tomography. *J Fluorine Chem,* 2006. 127: p. 1488-1493.

Lebedev, A., et al., Batch-reactor microfluidic device: first human use of a microfluidically produced radiotracer. *Lab Chip*, 2013. 13: p. 136.

Lee, J., et al., Preparation of Ultrafine Fe_3O_4 Particles by Precipitation in the Presence of PVA at High pH. *Journal of Colloid and Interface Science*, 1996. 177: p. 490–494.

Lee, J. and C.J. Kim, Liquid micromotor driven by continuous electrowetting. *Micro Electro Mechanical Systems*, 1998. MEMS 98: p. 538-543.

Lee, S.J., et al., Simple and highly efficient synthesis of 3'-deoxy-3'-[^{18}F]fluorothymidine using nucleophilic fluorination catalyzed by protic solvent. *Eur J Nucl Med Mol Imaging*, 2007. 34: p. 1406-1409.

Leo, A., et al., Partition coefficients and their uses. *Chem. Rev.*, 1971. 71: p. 525-616.

Liu, Y., et al., Multifunctional silica nanoparticles for targeted delivery of hydrophobic imaging and therapeutic agents. *International Journal of Pharmaceutics*, 2011. 421: p. 370– 378.

Liu, Z., et al., Rapid, one-step, high yielding 18F-labeling of an aryltrifluoroborate bioconjugate by isotope exchange at very high specific activity. *J Label Compd Radiopharm*, 2012. 55: p. 491-496.

Liu, Z., et al., Kit-like 18F-labeling of RGD-19F-Arytrifluroborate in high yield and at extraordinarily high specific activity with preliminary in vivo tumor imaging. *Nuclear Medicine and Biology*, 2013. 40: p. 841–849.

Lu, S., et al., Fluorine-18 chemistry in micro-reactors. *J labeled Compd Radiopharm.*, 2010. 53(5-6): p. 234-238.

Ma, M. et al., "A new bifunctional chelator for copper radiopharmaceuticals: a cage amine ligand with a carboxylate functional group for conjugation to peptides." *Chem Commun.*, 2009. p. 3237-3239.

Makhluf, S.B.D., et al., Modified PVA–Fe_3O_4 Nanoparticles as Protein Carriers into Sperm Cells. *Small*, 2008. 4(9): p. 1453–1458.

Mason, N.S. and C. A. Mathis, in Positron emission tomography: basic sciences, Springer, London; New York, 2005.

Massoud, T.F. and S.S. Gambhir, Integrating noninvasive molecular imaging into molecular medicine: an evolving paradigm. *Trends Mol. Med.*, 2007. 13: p. 183-91.

Matestic, L., et al., Ascertaining the suitability of arylsulfonyl fluorides for [18F]radiochemistry applications: A systematic investigation using microfluidics. *J. Org. Chem.*, 2013. 78: p. 11262-11270.

Moon, W.Y., et al., Simple purification of recovered [18O]H2O by UV, ozone, and solid-phase extraction methods. *Appl. Radiat. Isot.* 2007. 65: p. 635-640.

Morag, E., et al., Reversibility of biotin-binding by selective modification of tyrosine in avidin. *Biochem. J.*1996. 316: p. 193-199.

Miller, P.W., et al., Synthesis of 11C, 18F, 15O, and 13N radiolabels for positron emission tomography. *Angew. Chem., Int.* Ed., 2008. 47: p. 8998-9033.

Navari M., et al., Regioselective radiofluorodestannylation with [^{18}F]F_2 and [^{18}F]CH_3COOF: a high yield synthesis of 6-[^{18}F]fluoro-L-dopa. *Appl. Rad. Isot.*, 1992. 43(8): p. 989-996.

Overman, R.T. and H. M. Clark, Radioisotope techniques, McGraw-Hill, New York, 1960.

Pelizzari, C.A., et al., Accurate three-dimensional registration of CT, PET, and/or MR images of the brain. *J. Comput. Assist. Tomogr.*, 1989. 13: p. 20-26.

Price, E. and C. Orvig, Matching chelators to radiometals for radiopharmaceuticals. *Chem. Soc. Rev.*, 2014.43: p. 260

Rensch, C., et al., Microfluidics: A groundbreaking technology for PET tracer production? *Molecules*, 2013. 18 (7): p. 7930-7956.

Robinson, P.J., et al., The properties of magnetic supports in relation to immobilized enzyme reactors. *Biotechnol. Bioeng*. 1973. 15: p. 603.

Ross, T.L. and S. M. Ametamey, in Basic Sciences of Nuclear Medicine (Ed.: M. M. Khalil), Springer, Berlin; Heidelberg, 2011.

Saha, G.B., Physics and radiobiology of nuclear medicine, 3rd ed., Springer, New York, 2006.

Sathekge, M., et al., Use of 18F-FDG PET to predict response to first-line tuberculosis in HIV-associated tuberculosis. *J Nucl Med*, 2011. 52 (6) : p. 880-885

Schubiger, P.A., Lehmann, L., Friebe, M., Editors, PET Chemistry: The Driving Force of Molecular Imaging. [In: Ernst Schering Res. Found. Workshop; 2007, 62]. Springer,GmbH, 2007.

Schlyer, D.J., et al., Impurities in the [18O]water target and their effect on the yield of an aromatic displacement reaction with [18F]fluoride. *Appl. Radiat. Isot.*, 1993. 44: p. 1459-1465.

Sharma, S.P., et al., Whole-body PET acceptance test in 2D and 3D using NEMA NU 2-2011 protocol. *J Med Phys*. 2007. 32 (4): p. 150-155.

Shokeen, M. and C. J. Anderson, Molecular Imaging of Cancer with Copper-64 Radiopharmaceuticals and Positron Emission Tomography (PET). *Acc Chem Res*., 2009. 42 (7): p. 832-841.

Som, P., et al., A fluorinated glucose analog, 2-fluoro-2-deoxy-D-glucose (F-18): nontoxic tracer for rapid tumor detection. *J. Nucl. Med.,* 1980. 21: p. 670-675.

Sommer, H. and L. Jackson. Alkylation of Amines: A new method for the synthesis of quaternary ammonium compounds from primary and secondary amines. Edgewood Arsenal Technical Report (EATR 4311), Edgewood Arsenal, Maryland, 1969.

Svadberg, A. Nucleophilic substitution reactions for Positron Emission Tomography: Factors influencing the reactivity of [^{18}F]Fluoride (Doctoral thesis). University of Tromso, Norway, 2012.

Schirrmacher, E., et al., synthesis of p-(Ditert-butyl[18F]fluorosilyl) benzaldehyde ([18F]SiFA-A) with high specific activity by isotopic exchange: a convenient labeling synthon for the 18F-labeling of N-amino-oxy derivatized peptides. *Bioconjugate Chem*, 2007. 18: p. 2085-2089.

Thumshirn, G., et al., Multimeric cyclic RGD peptides as potential tools for tumor targeting: solid-phase peptide synthesis and chemoselective oxime ligation. *Chem. Eur. J., 2003. 9*: p. 2717–2725.

Ting, R., et al., Toward [18F]-labeled aryltrifluoroborate radiotracers: in vivo PET Imaging of stable aryltrifluoroborate clearance in mice. *J. Am. Chem. Soc.*, 2008. 130: p. 12045-12055.

Townsend, D.W., Combined PET/CT: the historical perspective. *Semin Ultrasound CT MR,* 2008. 29 (4): p. 232.-235.

Tredwell, M., et al., A General Copper-Mediated Nucleophilic ^{18}F Fluorination of Arenes. *Angew. Chem. Int. Ed.*, 2014. 53: p. 7751-7755.

Vlasov, V.M., Fluoride ion as a nucleophile and a leaving group in aromatic nucleophilic substitution reactions. *J. Fluorine Chem.*, 1993. 61: p. 193-216.

Voss, S., et al., Positron emission tomography (PET) imaging of neuroblastoma and melanoma with ^{64}Cu-SarAr immunoconjugates. *P Natl Acad Sci USA*, 2007. 104: p. 17489-17493.

Wang, M.W., et al., Microfluidics for Positron Emission Tomography Probe Development. *Molecular Imaging*, 2010. 9(4): p. 175-191.

Watts, P. and S.J. Haswell, The application of micro reactors for organic synthesis. *Chemical Society Reviews*, 2005. 34(3): p. 235-246.

Watts, P. and C. Wiles, Micro reactors: a new tool for the synthetic chemist. *Organic & Biomolecular Chemistry*, 2007. 5(5): p. 727-732.

Weissleder, R. and U. Mahmood, Molecular Imaging. *Radiology*, 2001. 219 (2): p. 316-333.

Welch, M. J. R. and C. S. Redvanly (Eds.), in Handbook of radiopharmaceuticals: radiochemistry and applications, Wiley, New York, 2003.

Wester, H.J., Munich Molecular Imaging Handbook Series Pharmaceutical Radiochemistry (I). Vol. 1. 2011: Scintomics. 212.

Williams, H., et al., A comparison of PET imaging characteristics of various copper radioisotopes. *Eur J Nucl Med Mol I*, 2005. 32: p. 1473-1480.

Wirth, T., Microreactors in organic synthesis and catalysis. 2008, Weinheim: Wiley-VCH. xiv, 283 p. 1,19, 43-53.

Woods, R.P., et al., MRI-PET registration with automated algorithm. *J. Comput. Assist. Tomogr.*, 1993. 17: p. 536-546.

Wrenn, F.R., et al., Use of positron-emitting radioisotopes for the localization of brain tumors. Science, Washington, DC, 1951. 113, p. 525-527.

Appendix: Data and Sample Calculations

A.1 Radioactivity decay correction

Radionuclides will undergo radioactive decay due to the disintegration of the unstable nuclei. The disintegration rate *dN*/*dt* (or disintegrations per second, dps) is referred to as the *radioactivity* or simply the *activity* of the radionuclide. The activity of a radionuclide (A) can be expressed as the number of disintegrations, proportional to the total number of nuclei present at that time as shown in Equation A.1.

Equation A.1 Activity of a radionuclide

$$A = -\frac{dN}{dt} = \lambda N$$

where *N* is the number of radioactive nuclei present, and *λ* is the *decay constant* of the radionuclide. One dps is equivalent to 1 Becquerel (Bq) which is the SI unit for activity. Another commonly used unit for activity is Curie (Ci) which is equivalent to 3.7×10^{10} Bq. Equation A.1 can then be expressed as an exponential equation (Equation A.2) indicating that the radioactivity decays exponentially. This is the equation used for decay correction in this thesis.

Equation A.2 Decay Correction Equation

$$\mathbf{A_t = A_0 e^{-\lambda t}}$$

where A_0 (mCi) is the activity at the end of bombardment (EOB) of the target material, A_t (mCi) is the activity measured at time t (min) after EOB and λ is the decay constant. A_t is the measured activity from the detector and A_o is the decay-corrected activity at EOB. This equation is used to calculate the decay-corrected activity of the data given in Table A.1.

Furthermore, every radionuclide is characterized by its *half-life* ($t_{1/2}$), which is the time it takes for the radioactive nuclides to decay by half of their amount. The half-life is related to the decay constant *λ* of a radionuclide by Equation A.3.

Equation A.3 Decay constant of a radionuclide

$$\lambda = 0.693/t_{1/2}$$

Table A.1 Radioactivity measured (A_t) at a specific time (*t*) and the decay corrected activity (A_0)

Half-life, $t_{1/2}$	Decay constant, λ	Radioactivity measured, A_t	Time from EOB, *t*	Decay-corrected Activity, A_0
109.77 min	0.00631 min^{-1}	0.81 mCi	131.24 min	1.86 mCi*

*This value is reported in Section 3.3, Table 3.2.

Sample Calculation for decay-corrected activity:

The rate constant for ^{18}F is calculated first by Equation A.3,

$\lambda = 0.693/t_{1/2} = 0.693/109.77 \text{ min} = 0.00631 \text{ min}^{-1}$

To calculate the activity at the end of bombardment (A_0), Equation A.2 is used:

$A_0 = 0.81 \text{ mCi} \times \exp[(0.00631 \text{ min}^{-1})(131.24 \text{ min})] = 1.86 \pm 0.02 \text{ mCi}$

The error reported on the above calculation is calculated from the propagated uncertainty in the radioactivity and the time measurement:

Relative uncertainty in radioactivity measurement = 0.01/0.81 = 0.0123

Relative uncertainty in exponent term = square root $\{[(6.31\times10^{-5})^2 + (3.77 \times 10^{-4})^2] \times 2.29^2\} = 9 \times 10^{-4}$

To calculate the error: square root $\{[(0.0123)^2 + (9 \times 10^{-4})^2] \times 1.86^2\} \approx 0.02$ mCi

A.2 Calculation of Capture Efficiency and Release Efficiency of Magnetic Particles

The capture and release efficiencies reported in this thesis (e.g. Section 3.3, Table 3.2 and 3.3; Section 3.4, Table 3.4; Section 3.5, Table 3.5) are calculated from the decay-corrected activity values. A sample calculation is shown for the data given in Table A.2. The data obtained from experiments are the initial activity (the initial activity

used per trial), activity measured in the waste (activity measured from the solution collected from the capillary tube) and the released activity (activity measured from the droplet collected after particles reacted with K_2CO_3).

Table A.2 Sample data for the calculation of capture and release efficiency

Data (Decay Corrected)	
Initial Activity	3.60 mCi
Activity in waste	0.79 mCi
Activity in released solution	2.64 mCi
Calculated Values	
activity captured in particles	2.810 mCi
Capture Efficiency	78.2%
Release Efficiency	93.8%

Sample calculation for capture and release efficiency:

Activity captured in particles = Initial activity – Activity in Waste = 3.60 mCi – 0.79 mCi

$$= 2.810 \pm 0.014 \text{ mCi}$$

Equation 3.1 is used to calculate capture efficiency:

Capture Efficiency = (Activity Captured/Initial Activity) x 100%

$$= (2.810 \text{ mCi}/3.60 \text{ mCi}) \times 100\% = 78.2 \pm 0.4\ \%$$

Equation 3.2 is used to calculate release efficiency:

Release Efficiency = [Released Activity/ (Initial activity – Activity in Waste)] x 100%

$$= (2.64\text{mCi}/2.810\text{mCi}) \times 100\% = 93.8 \pm 0.6\ \%$$

A.3 Calculation of Mass of fluoride ions from Radioactivity

The mass of fluoride ions reported in Table 3.2 and Table 3.3 is calculated from the measured radioactivity and the specific activity. The specific activity of [^{18}F]fluoride solution produced from TR-13 cyclotron at TRIUMF by irradiation of 1 mL of $H_2{}^{18}O$ usually gives a specific activity of 2 Ci/µmol (Füchtner et al, 2008). As an example,

Radioactivity = 1.86 mCi = 0.00186 Ci

To get the amount of of fluoride in µmol,

Amount of fluoride = (0.00186 Ci / 2 Ci/µmol) = 0.000930 µmol x (19 µg/µmol)

= 0.018 ± 0.008 µg F^- ions

A.4 Calculation of Radiochemical Yield (RCY)

The RCYs reported in Section 3.6, Table 3.6, are calculated using Equations 3.4 and 3.5. A sample calculation is performed using the data in Table A.3.

Table A.3 Sample Data for the calculation of radiochemical yield (RCY)

Data (Decay-Corrected)	
Initial Activity	3.84 mCi
Activity in waste	0.85 mCi
Released Activity in released solution	2.83 mCi
Radiochemical Purity (from HPLC data)	95.91%
Calculated RCY*	70.7 %

*The RCY calculated is reported on Table 3.6.

Sample calculation of RCY using Equation 3.5,

RCY % = { [2.83 x (95.91/100)] / 3.84 } x 100% = 70.7 ± 0.3 %

A.5 Specific Activity

A.5.1 Calibration Curve for Calculation of specific activity of [^{18}F]-(2)

As discussed in Section 2.5.1, [^{19}F]-(2) was dissolved in 10 mL MeCN to give a 2 mM solution. This stock solution was serially diluted into 3 solutions of different concentrations using MeCN. An aliquot (25 µL) of each solution was assayed by HPLC. For each solution, three injections were performed and the peak area of the compound was determined. The average of the three values was used to generate the calibration curve. Table A.4 shows the data for the calibration curve.

Table A.4 Data used to generate the calibration curve in Figure A.1

Concentration, nmol (X values)	Peak Area (Y values)
2.7	1695 ± 43
4.54	3179 ± 117
6.48	4629.9 ± 83

Errors are SD (n = 3)

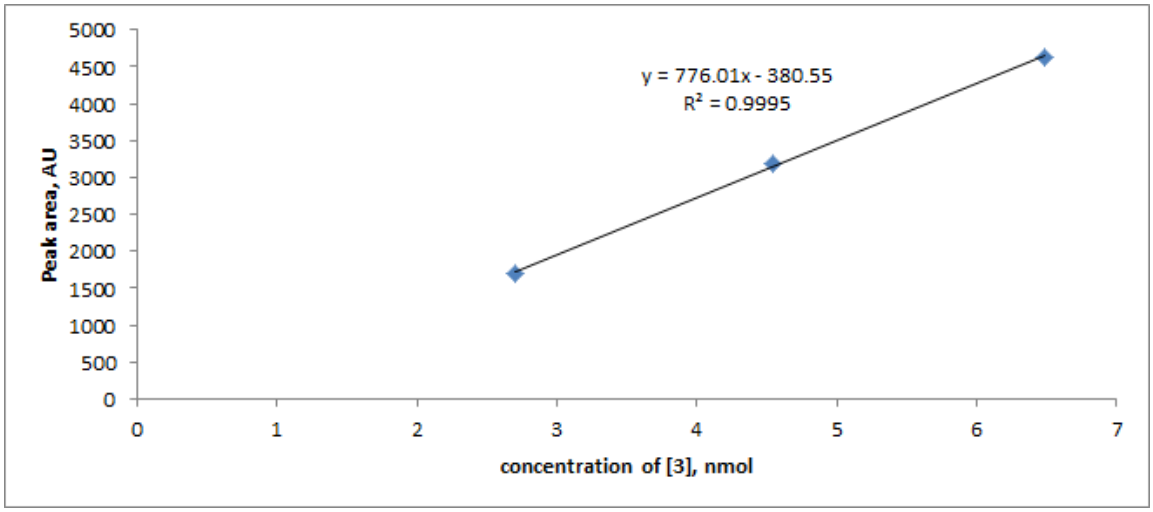

Figure A.1. Calibration curve using [^{19}F]-(2) as a standard solution

A.5.2 Calculation of Specific Activity of [^{18}F]-(2)

The activity values are used to calculate the specific activity (SA) which is the ratio of the activity (Ci) of a radiolabeled compound to the mass of its non-radioactive counterpart, plus the radioactive component (relatively small). Table A.5 shows the radioactivity of the product collected, the peak area obtained from a 40 µL aliquot, and the corresponding specific activity of the product.

Table A.5 Data for the calculation of specific activity of product produced using the MDM method

	Data obtained from experiment		Calculated Values	
Trial	**Radioactivity (Ci) of the total product mixture collected (100 µL)**	**Peak Area of product in a 40 µL aliquot**	**Specific Activity in Ci/µmol**	**Specific Activity in Gbq/µmol**
1	0.00193	54.0	1.4	51.8
2	0.00184	77.3	1.3	48.1
3	0.00182	92.8	1.2	44.4

The linear equation obtained through the calibration curve (Figure A.1) was then used to calculate the number of moles of product present in the sample. Table A.5 shows the data used to calculate the specific activity.

A sample calculation is shown below for the specific activity reported in Table A.5, trial 1:

x = (y + 380.55)/776.01 = (54.0 + 380.55)/776.01 = 0.56 nmol ± 0.11

= 0.000560 µmol for every 40 µL sample injected

To calculate the amount of product (µmol) in the total sample (100 µL):

(0.000560 µmol/40 µL) x 100 µL = 0.0014 µmol ± 0.0003

Given the activity of the total sample (100 µL) = 0.00193 Ci,

Specific activity = 0.00193 Ci/0.0014 µmol = 1.4 ± 0.3 Ci/µmol

Since 1 Ci = 37 GBq, then 1.4 Ci/µmol can be converted to 51.8 ± 0.3 GBq/µmol

A.6 [^{18}F]fluoride Release Efficiency with Cs_2CO_3 and $NaClO_4$

For the synthesis of [^{18}F]-(2), a solution of Cs_2CO_3 was used by Inkster et al. (2012) to elute [^{18}F]F^- ions from the anion-exchange column. It was discussed that Cs_2CO_3 was used since it is better at promoting SN2-type fluorination reactions, owing to the enhanced solubility of CsF in alcoholic solvents and CsF nucleophilicity. On the other hand, for the synthesis of [^{18}F]-(5), a solution of $NaClO_4$ was used by Liu et al. (2012) as the releasing solution, since its pH is neutral while that of K_2CO_3 solution is basic (as discussed in Section 3.7).

Therefore, three releasing solutions (K_2CO_3, Cs_2CO_3 and $NaClO_4$) were tested. The release efficiency of these solutions for the magnetic particles was determined. For each type of solution, it was observed that the lower the concentration of the releasing solution, the lower is the release efficiency. For a concentration of 0.145 M, the average release efficiency for Cs_2CO_3 was slightly lower than K_2CO_3. But one must note that the standard deviation is high, which means that the release efficiency could vary considerably per trial. In the case of $NaClO_4$, a lower release was achieved since lower $NaClO_4$ concentrations were used to avoid safety issues considering that it is a strong oxidant.

Table A.6 Release efficiency of [^{18}F]fluoride ions trapped on QMA-tagged magnetic particles with Cs_2CO_3, $NaClO_4$ and K_2CO_3

	Concentration, M	Release Efficiency, %
K_2CO_3	0.0774	82 ± 2 (n=3)
	0.145	93 ± 4 (n=5)
Cs_2CO_3	0.0252	30 ± 4 (n=3)
	0.145	86 ± 5 (n=6)
$NaClO_4$	0.0163	6 ± 1 (n=3)
	0.0817	58 ± 4 (n=4)

Sample calculation of release efficiency is shown on Appendix, Section A.2. All activity values are decay-corrected to EOB and errors are SD.